Molecular Neurobiology
https://doi.org/10.1007/s12035-022-03049-1

Function of FMRP Domains in Regulating Distinct Roles of Neuronal Protein Synthesis

Michelle Ninochka D'Souza[1,2,3] · Sarayu Ramakrishna[1,2,3] · Bindushree K. Radhakrishna[3] · Vishwaja Jhaveri[1] · Sreenath Ravindran[1] · Lahari Yeramala[4] · Deepak Nair[5] · Dasaradhi Palakodeti[1] · Ravi S. Muddashetty[3]

Received: 11 January 2022 / Accepted: 9 September 2022

Abstract

The Fragile-X Mental Retardation Protein (FMRP) is an RNA binding protein that regulates translation of mRNAs essential for synaptic development and plasticity. FMRP interacts with a specific set of mRNAs, aids in their microtubule-dependent transport and regulates their translation through its association with ribosomes. However, the biochemical role of FMRP's domains in forming neuronal granules and associating with microtubules and ribosomes is currently undefined. We report that the C-terminus domain of FMRP is sufficient to bind to ribosomes akin to the full-length protein. Furthermore, the C-terminus domain alone is essential and responsible for FMRP-mediated neuronal translation repression. However, dendritic distribution of FMRP and its microtubule association is favored by the synergistic combination of FMRP domains rather than individual domains. Interestingly, we show that the phosphorylation of hFMRP at Serine-500 is important in modulating the dynamics of translation by controlling ribosome association. This is a fundamental mechanism governing the size and number of FMRP puncta that contain actively translating ribosomes. Finally through the use of pathogenic mutations, we emphasize the hierarchical contribution of FMRP's domains in translation regulation.

Keywords FMRP · Fragile X Syndrome · Translation regulation · Phosphorylation · Neuronal granules · Microtubules · Ribosomes

✉ Ravi S. Muddashetty
ravimshetty@iisc.ac.in

Michelle Ninochka D'Souza
michellend@instem.res.in

Sarayu Ramakrishna
sarayur30@gmail.com

Bindushree K. Radhakrishna
bindushree2705@gmail.com

Vishwaja Jhaveri
vishwaja.jhaveri95@gmail.com

Sreenath Ravindran
sreenathlnx@gmail.com

Lahari Yeramala
ylahari@gmail.com

Deepak Nair
deepak@iisc.ac.in

Dasaradhi Palakodeti
dasaradhip@instem.res.in

[1] Institute for Stem Cell Science and Regenerative Medicine, Bangalore, India 560065

[2] The University of Trans-Disciplinary Health Sciences and Technology (TDU), Bangalore, India 560064

[3] Centre for Brain Research, Indian Institute of Science, CV Raman Avenue, Bangalore, India 560012

[4] National Centre For Biological Sciences, Tata Institute of Fundamental Research, Bangalore, India 560065

[5] Centre for Neuroscience, Indian Institute of Science, Bangalore, India 560012

Published online: 01 October 2022

Introduction

Fragile X Syndrome (FXS) is a trinucleotide repeat expansion disorder of the *FMR1* gene resulting in intellectual disability [1]. The silencing of the gene due to the expansion of CGG repeat in its 5′UTR results in the loss of the encoded protein Fragile X Mental Retardation Protein (FMRP). FMRP is an RNA binding protein, structurally comprising of protein interacting Tudor and KH0 domains and two types of RNA binding domains: two K Homology (KH) domains and one RGG domain in the intrinsically disordered C-terminus [2–5]. FMRP is implicated in a range of biological processes such as chromatin remodeling, ion channel stability, RNA transport, ribosome heterogeneity and translation regulation [6–12]. However, the contribution of FMRP to FXS pathology is mostly studied in the absence of the protein and the role of the individual domains of FMRP in these cellular processes is yet to be investigated.

FMRP plays a key role in maintaining synaptic development and plasticity through regulation of protein synthesis [13, 14]. FMRP is primarily shown to act as a translational repressor [15]. However, FMRP also activates the translation of specific candidates both on mGluR and NMDAR stimulation [10, 11]. It is important to note that FMRP-bound targets localize to neuronal processes in the form of granules in a microtubule-dependent manner [16] and the expression of these targets is guided through FMRP's distribution to polysomes [17–19]. The interaction of FMRP with ribosomes seems to be an important prerequisite for this. An added level of translation regulation lies in the phosphorylation of FMRP. Phosphorylation of hFMRP, primarily at Serine-500, is shown to influence the bidirectional role of FMRP as a regulator of synaptic protein synthesis [20–23].

The function of FMRP comprises the multistep process of granule formation, association with microtubules, and interaction with ribosomes. Only a few studies address the mechanism of these interactions through truncations and mutations of FMRP. The N-terminus domain of FMRP is shown to modulate the expression and activity of several ion channels [24, 25] while the RGG domain in the C-terminus is implicated in RNA binding and consequent gene expression [26, 27]. Further, the *I304N* mutation of FMRP, which results in a severe form of FXS, illustrates the importance of KH domains in polysome association and translation regulation [18, 28]. Apart from *I304N*, gene sequencing studies have uncovered a series of other mutations in *FMR1* leading to FXS-like phenotypes. In silico analysis of *FMR1* SNPs indicate that *R138Q* mutation in the NLS of FMRP alters the localization of FMRP without any structural effect on the protein [2, 29]. But, mutations in the KH domains like *G266E* and *I304N* seem to disturb the interactions between domains, disrupting the overall structure and function of FMRP [29, 30]. C-terminus domain mutations such as *R534H* and *G482S* have been predicted to alter RNA binding and recognition [31]. In addition, the frame shift mutation (*G538fs*23*) in the open reading frame of FMRP has been shown to introduce novel sequences, which drastically alter the cellular localization of FMRP [32]. These mutational studies emphasize the probable structural defects and the contribution of individual domains of FMRP. However, the consequence of these point mutations in cellular processes is yet to be addressed. Further, this has generated a vacuum in the information available to understand the functions manifested by FMRP mutants.

The function of FMRP is complex and studying the role of individual domains and their synergistic effect is beneficial in understanding FMRP-mediated regulation of protein synthesis. Here, we systematically investigate the contribution of FMRP and its domains in the dynamic processes of (i) ribosome binding (ii) mRNP granule formation and (iii) microtubule association. Our results provide structural insights on the importance of the C-terminal domain in ribosome binding and subsequent regulation of neuronal translation. We also emphasize the role of phosphorylation of FMRP in the formation of granules and their association with microtubules. Our findings elucidate the functional consequences of pathogenic point mutations on regulatory mechanisms of FMRP. This is important to understand FMRP domains and their role in coordinating the mechanisms leading to translation regulation.

Methods

Animals

Sprague–Dawley (SD) rats were used in all animal experiments. Rodents were maintained at conditions with 20–22 °C temperatures, 50–60 relative humidity, 0.3 µm-HEPA-filtered air supply at 15–20 ACPH, and 14-h/10-h light dark cycle was maintained.

Cell Line and Primary Neuronal Cultures

HEK293T cells were a gift from Dr. Dasaradhi Palakodeti, InStem. HEK293T cells were cultured in Dulbecco's Modified Eagle Medium (#21,331–020 Thermo) containing 10% fetal bovine serum (#F2442 Sigma) at 37 °C and 5% CO_2. Cells were passaged with 0.25% trypsin solution (#15,090,046 Thermo) for 2 min and neutralized using the same culture medium. Primary neuronal cultures were obtained from E18 rat embryos. Primary cultures

were processed as previously described [10]. Briefly, cortices from both the hemispheres were dissected out from E18 embryos in ice cold Hank's balanced salt solution (#H6648-1L Sigma). The tissue was incubated with 0.25% Trypsin solution for 5 min at 37 °C to enzymatically dissociate the cells and finally manually triturated in Minimum Eagles Medium (#11,095,080 Thermo) containing 10% FBS (#F2442 Sigma) to generate a single cell suspension. Cells were plated at a density of 6×10^4 cells/cm^2 on glass coverslips coated with 0.2 mg/ml poly-L-lysine (#P2636-100MG Sigma) made in Borate buffer pH 8.5. Neurons were cultured in MEM medium for 4 h after plating following which they were cultured in neurobasal medium (#21,103–049 Thermo) containing B27 supplement (#17,504–044 Thermo) and 1 × Glutamax (#35,050,061 Thermo) for 11 days at 37 °C and 5% CO_2.

Cloning and Site-Directed Mutagenesis

In plasmids generated for cell line and neuronal transfection, all truncations and site-directed mutations (SDM) of FMRP were performed in the original plasmid pFRT-TODestFLAGHAhFMRPiso1 (#48,690 Addgene) containing full-length human FMR1 gene with N-terminal Flag-HA tag. Site-directed mutagenesis was performed using overlapping PCR with Phusion® high-fidelity DNA polymerase (#M0530S NEB) and primer sequences mentioned in Table 1. Plasmids generated for recombinant protein were constructed as follows. Sequences corresponding to N-terminus (1-216aa), KH (217-425aa), and C-terminus (426-632aa) were PCR amplified from plasmid pFRT-TODestFLAGHAhFMRPiso1 and cloned into PGEX6P1 vector (#GE28-9546–48 Cytiva) with N-terminus GST tag and PreScission protease site. Full-length FMR1 sequence was PCR amplified along with N-terminal 6XHis tag and cloned into PFastBac-HtB (#10,712,024 Thermo) for baculoviral protein expression.

Over-expression and Protein Purification Experiments

For transfections, HEK293T cells/DIV11 primary neurons were transfected with Flag-HA-tagged FMRP constructs using Lipofectamine 2000 (#11668027 Thermo) for 24 h as per the reagent's protocol. His-GFP was also used as a control and transfection was performed in a similar manner as mentioned before. All constructs were transfected at equal concentrations. Flag-HA FMRP G538fs*23 showed very less transfection efficiency and hence was doubled in concentration with every transfection (Fig. S5a-c).

The N-terminus (1-216aa), KH (217-425aa), and C-terminus (426-632aa) of FMRP bearing GST tag at the N-terminal was transformed into *Escherichia coli* (*E. coli*) Rosetta DE3 cells and grown at 37 °C in LB. Protein expression was induced with 0.5 mM IPTG at an OD600nm ~ 0.6 and

Table 1 Primer details for SDM and qPCR

Primer	Sequences
SDM I304N forward	GAAAGCTGAATCAGGAGATTGTGGAC
SDM I304N reverse	CTCCTGATTCAGCTTTCCATTTTTTC
SDM R138Q forward	GTGCCAGAAGACTTACAACAAATGTGTG
SDM R138Q reverse	CACACATTTGTTGTAAGTCTTCTGGCAC
SDM I241N forward	GCTAATAATCAGCAAGCTAGAAAAGTACC
SDM I241N reverse	CTGATTATTAGCACCATGAGTACC
SDM S500D forward	CAAATGCTGACGAAACAGAATCTGACCAC
SDM S500D reverse	CTGTTTCGTCAGCATTTGATGCTTCAG
SDM S500A forward	CAAATGCTGCAGAAACAGAATCTGACCAC
SDM S500A reverse	CTGTTTCTGCAGCATTTGATGCTTCAG
SDM G266E forward	CATATTTATGAAGAGGATCAGGATGCAGTG
SDM G266E reverse	GATCCTCTTCATAAATATGAAATGTGCAGGTATC
SDM G482S forward	GGGGGCACTCTAGACGCGGTCCTG
SDM G482S reverse	CGTCTAGAGTGCCCCCTATTTCTG
SDM G532fs*23 forward	TCCTCTTCCTCCCCCCTCCAC
SDM G532fs*23 reverse	GGGAGGAAGAGGACAAGGAG
SDM R534H forward	ACGGCGGCATGGAGGGGGAGG
SDM R534H reverse	CCTCCATGCCGCCGTCCGTCTC
18S rRNA forward	CAAGACGGACCAGAGCGAAAG
18S rRNA reverse	GAGCCATTCGCAGTTTCA
28S rRNA forward	GAACCTGGCGCTAAACCATTCG
28S rRNA reverse	CCCTTGTGTCGAGGGCTGAC

grown overnight at 25 °C. Cells were harvested and pelleted via centrifugation. Pellets were stored at − 20 °C or used immediately. Cells were lysed in buffer containing 20 mM Tris pH 8, 500 mM KCl, and 1 mM DTT and sonicated for 30 min (10 s ON, 10 s OFF). Lysed cells were spun down and lysate was then loaded on to glutathione sepharose beads equilibrated with lysis buffer. Resin was washed with 10 column volumes of lysis buffer followed by 5 column volumes of lysis buffer with 100 mM KCl. Elution buffer containing 50 mM Tris pH 8, 100 mM KCl, 1 mM DTT, 10% glycerol, and 10 mM reduced glutathione was used to elute the GST-tagged domains of FMRP. The flow-through was concentrated and further purified using a Superdex 75 column (GE Healthcare) equilibrated with buffer containing 50 mM Tris pH 8, 100 mM KCl, 1 mM DTT, and 10% glycerol. Protein containing fractions were pooled together. The purity of protein was confirmed with SDS-PAGE gel.

Full-length FMRP was cloned into baculoviral pFastHTb vector with His-tag located towards the N-terminus of the protein. Sf9 insect cells were transfected with the construct with PEI and maintained at 26 °C at 120 rpm in SF900II medium (#10902088 Thermo) until virus supernatant P0 was harvested 5 days post-transfection. Cell number, viability, and diameter of the cells were monitored for baculoviral infection. P1 virus supernatant was further harvested from a larger scale culture. P1 virus was used to infect a fresh culture of Sf9 cells. The extent of baculoviral infection was monitored by recording the cell number, viability, and diameter prior to harvesting of cells. Cells were lysed in buffer containing 20 mM Tris pH7.5, 800 mM KCl, 5 mM BME, 10% glycerol, and 10 mM imidazole and sonicated for 1 min (10 s ON, 10s OFF). Lysed cells were spun down and lysate was loaded on to Ni–NTA beads equilibrated with lysis buffer. Resin was washed with 10 column volumes of lysis buffer followed by 5 column volumes of lysis buffer. His-FMRP was eluted in buffer containing 20 mM Tris pH7.5, 100KCl, 5 mM β-ME, 10% glycerol, and 100 mM imidazole. The flow-through was further dialyzed in the same buffer to eliminate imidazole.

Metabolic Labelling

For metabolic labelling of transfected neurons, neurons were incubated in methionine-free Dulbecco's Modified Essential Medium (#21013024 Thermo) for 30 min followed by addition of azidohomoalanine (AHA; 1 μM #C10102 Thermo) in the same medium. This was incubated for 30 min further and later fixed with 4%PFA. Cells were then permeabilized in PBS + 0.3% Triton X-100 solution and blocked with buffer containing PBS + 0.1% Triton X-100 + 2%BSA + 4% FBS solution. Newly synthesized proteins were then labelled with Alexa-Fluor-555–alkyne [Alexa Fluor 555 5-carboxamido-(propargyl), bis (triethylammonium salt)], by allowing the fluorophore alkyne to react with AHA azide group through click chemistry. All reagents were from Thermo Fisher, and stoichiometry of reagents was calculated according to the manufacture manual (#C10269 CLICK-iT cell reaction buffer kit).The neurons were subjected to immunostaining for MAP2B to identify neurons and HA to identify FMRP transfections (antibody details in Table 3). The coverslips were mounted with Mowiol® 4–88 mounting media (#81,381 Sigma) and imaged on Olympus FV3000 confocal laser scanning inverted microscope with 60 × objective. The pinhole was kept at 1 airy unit and the optical zoom at 2 × to satisfy Nyquist's sampling criteria in XY direction. The objective was moved in Z-direction with a step size of 1 μM (~ 8–10 Z-slices) to collect light from the planes above and below the focal plane. The transfected neurons were identified using the HA channel. Images of transfected and untransfected neurons were taken from each coverslip of every biological replicate. The image analysis was performed using ImageJ software and the maximum intensity projection of the slices was used for quantification of the mean fluorescent intensities. The region of interest (ROI) was drawn around transfected and untransfected neurons using the MAP2 channel for their respective analyses. The mean fluorescent intensity of the FUNCAT channel was normalized to the MAP2 channel for each ROI. For each construct, the FUNCAT/MAP2 intensity ratio of the transfected neurons was normalized to the untransfected neurons from the corresponding biological replicate. Data is represented as box plots indicating the quantification of the FUNCAT fluorescent intensity normalized to MAP2 fluorescent intensity. The box extends from 25th to 75th percentiles with the middlemost line representing the median of the dataset. Whiskers range from minimum to maximum data point.

Linear Sucrose Density Centrifugation

Polysome assay was done from HEK293T cell lysate as described previously in [10]. In brief, HEK293T cell lysate was separated on 15–45% linear sucrose gradient in presence of 0.1 mg/ml cycloheximide (CHX) and phosphatase inhibitor (#4906837001 Roche) by centrifugation at 39,000 rpm in SW41 rotor for 90 min. The sample was fractionated into 12 1.0 mL fractions with continuous UV absorbance measurement (A254). Fractions were further analyzed by Western blots. For quantification of FMRP distribution, Fractions were pooled (F1-2, F3 and F4–12) according to subunit distribution based on RPLP0 and RPS6 immunoblotting. Similar protocol was followed with purified recombinant full-length and domains of FMRP. 150 pmol of recombinant protein was spiked into pre-cleared HEK293T cell lysate and incubated for 10 min on ice prior to separation on sucrose gradient. Distribution of spiked/overexpressed proteins were quantified and bar graphs indicate the distribution of protein

Table 2 Antibodies for Western blot

Antibody	Dilution	Catalog no
GST	1:1000	Ab9085, Abcam
6His-Tag	1:3000	SAB4301134, Sigma
HA	1:1000	3724S, CST
RPS6	1:3000	2217S, CST
RPLP0	1:3000	Ab101279, Abcam
FMRP	1:1000	F4055, Sigma
p-FMRP	1:1000	Ab183319, Abcam
α-Tubulin	1:3000	T9026, Sigma
Secondary Rabbit HRP	1:5000	A0545, Sigma
Secondary Mouse HRP	1:5000	31430, Thermofisher Scientific

among mRNP (fractions 1–2), ribosomal subunits (fraction 3) and ribosomal fractions (fractions 4–12).

Binding Assays

A total of 50 pmol of recombinant GST-tagged domains of FMRP were incubated with pre-cleared HEK293T cell lysate. Ribosome protein complexes were formed for 30 min on ice and later incubated with 10 µl of GST-Sepharose beads for 2 h at 4 °C. After incubation, beads were pelleted (30 s at 1000 rpm). The beads were then washed twice with 50 µl of ice-cold binding buffer (20 mM HEPES pH7.5, 1 mM DTT, 100 mM KCl, 2.5 mM $MgCl_2$, and 10% glycerol). The amount of ribosome in cell lysate bound to beads was eluted with 1X Lamelli buffer and checked on a Western blot. Ribosomes from HEK293T cells were purified as described in Khatter et al. [33]. A total of 5 pmol of purified 80S were incubated with 50 pmol of recombinant protein in 50 µl of Binding buffer for 30 min on ice. Ribosome-protein complexes were incubated with 10 µl of GST-Sepharose beads for 2 h at 4 °C, eluted, and quantified as mentioned previously. For quantification of rRNA, Trizol (#15596018 Thermo) was added to the beads after the last wash and RNA was eluted as per manufacturer's protocol. Total RNA was reverse transcribed into cDNA using MMLV (#M0253L NEB) reverse transcriptase enzyme and random hexamers.

Quantitative PCR

rRNA was quantified using specific primers (Table 1) designed against human 18SrRNA and 28SrRNA. Arbitrary copy numbers were calculated from a standard curve drawn from Ct values obtained from serial dilutions of cDNA for each candidate.

Microtubule Enrichment Assay

To separate microtubule polymers from free tubulin, HEK293T cells were treated with 10 nM paclitaxel (#PHL89806-10MG Sigma) for 1 h to stabilize microtubules. Cells were later lysed in buffer containing 150 mM KCl, 2 mM MgCl2, 50 mM Tris, pH 7.5, 2 mM EGTA, 2% glycerol, 10 nM paclitaxel, 0.125% Triton X-100, protease inhibitor cocktail (#S8830-20TAB Sigma), and 10 U of RNase-out (#10777019 Thermo) at room temperature for 5 min. To analyze microtubule association of the Flag-HA-tagged wild-type and mutant FMRP variants, HEK293T cells were transfected with these constructs 24 h prior to paclitaxel treatment. For RNase treatment, the lysate buffer contained 1.2 µg/µl RNase A1 and 30 units of RNase T1 but no RNase-out. Nuclei were pelleted at 700 g for 1 min at room temperature and the cytoplasmic supernatant was centrifuged for 10 min at 16,000 g at room temperature to pellet microtubule polymers. The microtubule pellet and the post microtubule supernatant were denatured in 1 × Laemmli buffer followed by SDS-PAGE analysis. For microtubule-destabilizing experiments, HEK293T cells were incubated with 2 µg/ml nocodazole (#M1404 Merck) for 15 min prior to lysis with the same buffer containing nocodazole and no paclitaxel. Data is represented as box plots indicating the enrichment of overexpressed FMRP variants in the pellet/supernatant on Taxol treatment of HEK293T cells. The box extends from 25th to 75th percentiles with the middlemost line representing the median of the dataset. Whiskers range from minimum to maximum data points.

Western Blotting

The elutes from in vitro binding pull-downs, fractions of polysome profiling experiments, and fractions from microtubule enrichment assay were analyzed through Western blotting. Briefly, the denatured lysates were run on 12% resolving and 5% stacking acrylamide gels and subjected to overnight transfer on to PVDF membrane. The blots were subjected to blocking for 1 h at room temperature using 5% BSA prepared in TBST (TBS with 0.1% Tween-20). This was followed by primary antibody (prepared in

Table 3 Antibodies for immunostaining

Antibody	Dilution	Catalog no
MAP2	1:500	Ab32454, Sigma
HA	1:500	3724S, CST
Alexa Fluor 647 anti-mouse IgG	1:1000	A-21235, Thermofisher Scientific
Alexa Fluor 488 anti-rabbit IgG	1:1000	A-11008, Thermofisher Scientific

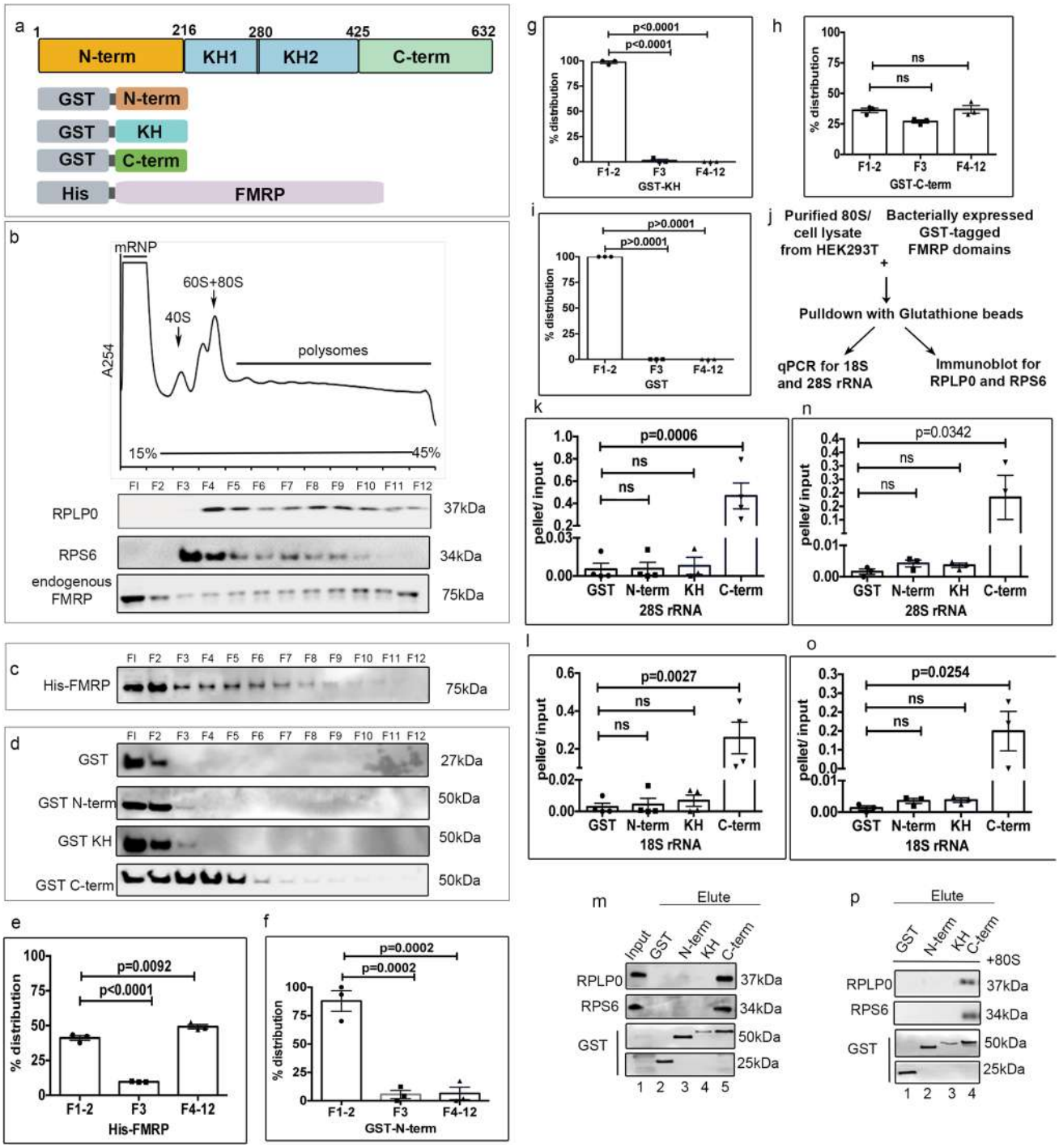

blocking buffer) incubation at 4 °C overnight. HRP-tagged secondary antibodies were used for primary antibody detection. The secondary antibodies (prepared in blocking buffer) were incubated with the blots for 1 h at room temperature. Three washes of 5–10 min each were given after primary and secondary antibody incubation using TBST solution. The blots were subjected to chemiluminescent-based detection of the HRP-tagged proteins. For the analysis of microtubule enrichment, the samples were probed with FMRP/GFP/HA antibody followed by α-tubulin as the loading control. In cases where the overexpressed protein shared the same molecular weight as α-tubulin, the blots were probed with FMRP/GFP/HA antibody first. The same blots were stripped and re-probed with α-tubulin antibody later. For sucrose gradient fractions, distribution of overexpressed protein and RPLP0/RPS6 was analyzed from the same blot. The details of the antibodies used and their dilutions are given in Table 2. All Western blot

◂**Fig. 1** C-terminus of FMRP is important for binding to ribosomes. **a** Schematic of the constructs for individual domains and full-length human FMRP. The GST-tagged domains and His-tagged full-length FMRP were expressed in bacteria and Sf9 insect cells respectively. Purified proteins were spiked into HEK293T cell lysate and subjected to polysome profiling on a linear sucrose gradient. **b** Top – representative polysome trace of HEK293T cell lysate on 15–45% linear sucrose gradient. Bottom – representative immunoblots for endogenous FMRP, RPLP0, and RPS6 distribution in the 12 fractions obtained from polysome profiling $n=3$. **c** Representative immunoblot for spiked His-tagged full-length FMRP distribution in the 12 fractions obtained from polysome profiling probed with anti-His antibody $n=3$. **d** Representative immunoblots indicating the distribution of spiked GST-tagged FMRP domains and purified GST in the 12 fractions obtained from polysome profiling. Blots were probed with anti-GST antibody $n=3$. **e** Graph indicating the quantification of His-FMRP among the mRNP (F1–2), ribosomal subunits (F3) and ribosomal fractions (F4–12). $n=3$. One-way ANOVA $p<0.0001$ with Dunnett's multiple comparison test. **f** Graph indicating the quantification of GST-N-term among the mRNP (F1–2), ribosomal subunits (F3), and ribosomal fractions (F4–12) $n=3$. One-way ANOVA $p=0.0001$ with Dunnett's multiple comparison test. **g** Graph indicating the quantification of GST-KH among the mRNP (F1-2), ribosomal subunits (F3), and ribosomal fractions (F4–12) $n=3$. One-way ANOVA $p<0.0001$ with Dunnett's multiple comparison test. **h** Graph indicating the quantification of GST-C-term among the mRNP (F1–2), ribosomal subunits (F3), and ribosomal fractions (F4–12), $n=3$. One-way ANOVA $p=0.0373$ with Dunnett's multiple comparison test. **i** Graph indicating the quantification of GST among the mRNP (F1–2), ribosomal subunits (F3) and ribosomal fractions (F4–12) $n=3$. One-way ANOVA $p<0.0001$ with Dunnett's multiple comparison test. **j** Experimental workflow to validate the binding of FMRP domains to ribosomes. **k** qPCR quantification of 28SrRNA from HEK293T cell lysate bound to GST-tagged FMRP domains. $n = 3$–4. Data represented as mean ± SEM, One-way ANOVA $p=0.0004$ with Dunnett's multiple comparisons test. **l** qPCR quantification of 18SrRNA from HEK293T cell lysate bound to GST-tagged FMRP domains. $n = 4$. Data represented as mean ± SEM, One-way ANOVA $p=0.0020$ with Dunnett's multiple comparisons test. **m** Representative immunoblots for RPLP0 and RPS6 obtained from pull-downs with GST-tagged FMRP domains incubated with HEK293T cell lysate ($n=2$). **n** qPCR quantification of 28SrRNA from purified 80S ribosomes bound to GST-tagged FMRP domains. $n = 4$. Data represented as mean ± SEM, One-way ANOVA $p=0.0332$ with Dunnett's multiple comparisons test. **o** qPCR quantification of 18SrRNA from purified 80S ribosomes bound to GST-tagged FMRP domains. $n = 3$–4. Data represented as mean ± SEM, One-way ANOVA $p=0.0244$ with Dunnett's multiple comparisons test. **p** Representative immunoblots for RPLP0 and RPS6 obtained from pull-downs with GST-tagged FMRP domains incubated with purified HEK293T 80S ribosomes ($n=2$)

quantifications were performed using densitometry analysis on ImageJ software.

Puncta Analysis

Rat primary cortical neurons were transfected with HA-FMRP constructs on DIV11 followed by fixation with 4% PFA on DIV12. In case of puromycin treated conditions, transfected neurons were incubated with puromycin (1 mM) for 1h at DIV 12. The fixed neurons were subjected to immunostaining for MAP2 and HA (antibody details in Table 3). The coverslips were mounted with Mowiol® 4–88 mounting media (#81381 Sigma) and imaged on Olympus FV300 confocal laser scanning inverted microscope with 60 × objective. The pinhole was kept at 1 airy unit and the optical zoom at 2 × to satisfy Nyquist's sampling criteria in XY direction. The objective was moved in Z-direction with a step size of 0.5 µM (~ 8–10 Z-slices) to collect light from the planes above and below the focal plane. The images were analyzed using ImageJ software and the maximum intensity projection of the slices was used for quantification. The MAP2 channel was used to draw the ROI around each dendritic segment and subjected to thresholding. The ROI created using the MAP2 channel was selected on the HA-FMRP image. The area selected ROI in the HA-FMRP channel was measured to obtain the total area of the dendritic ROI (a). Further, the ROI was subjected to particle analysis in the HA-FMRP image. Particles in the range of 3–30 pixels were considered for the analysis. The sum of the area of all the particles or the puncta area (b) and the number of particles or puncta (c) were the two parameters obtained using particle analysis. The ratio of puncta area (b) to total area (a) was calculated to measure the area occupied by the puncta in the given ROI. The ratio of puncta number (c) to total area (a) was calculated to measure the number of puncta per μm^2. The ratios of puncta area/total area and number of puncta/μm^2 were represented as box plots and compared among dendritic segment ROIs expressing different FMRP constructs. The box extends from 25th to 75th percentiles with the middlemost line representing the median of the dataset. Whiskers range from minimum to maximum data points.

Colocalization Analysis

For colocalization, cortical neurons were co-transfected with RPL10-GFP and HA-FMRP simultaneously at DIV11 followed by puromycin (1 mM) treatment at DIV12 for 1 h. The images were analysed using ImageJ software and the maximum intensity projection of the slices was used for quantification. The ROI was created using the MAP2 channel and was selected on the HA-FMRP image. Particle analysis was conducted on the selected ROI to identify the FMRP puncta. The mean intensity of FMRP and RPL10 was measured in these punctae. The mean intensity of FMRP and RPL10 in the puncta was normalized to the total intensity of FMRP and RPL10 in the ROI respectively. Data is represented as scatter plot that includes normalised FMRP intensity on X-axis and normalised RPL10

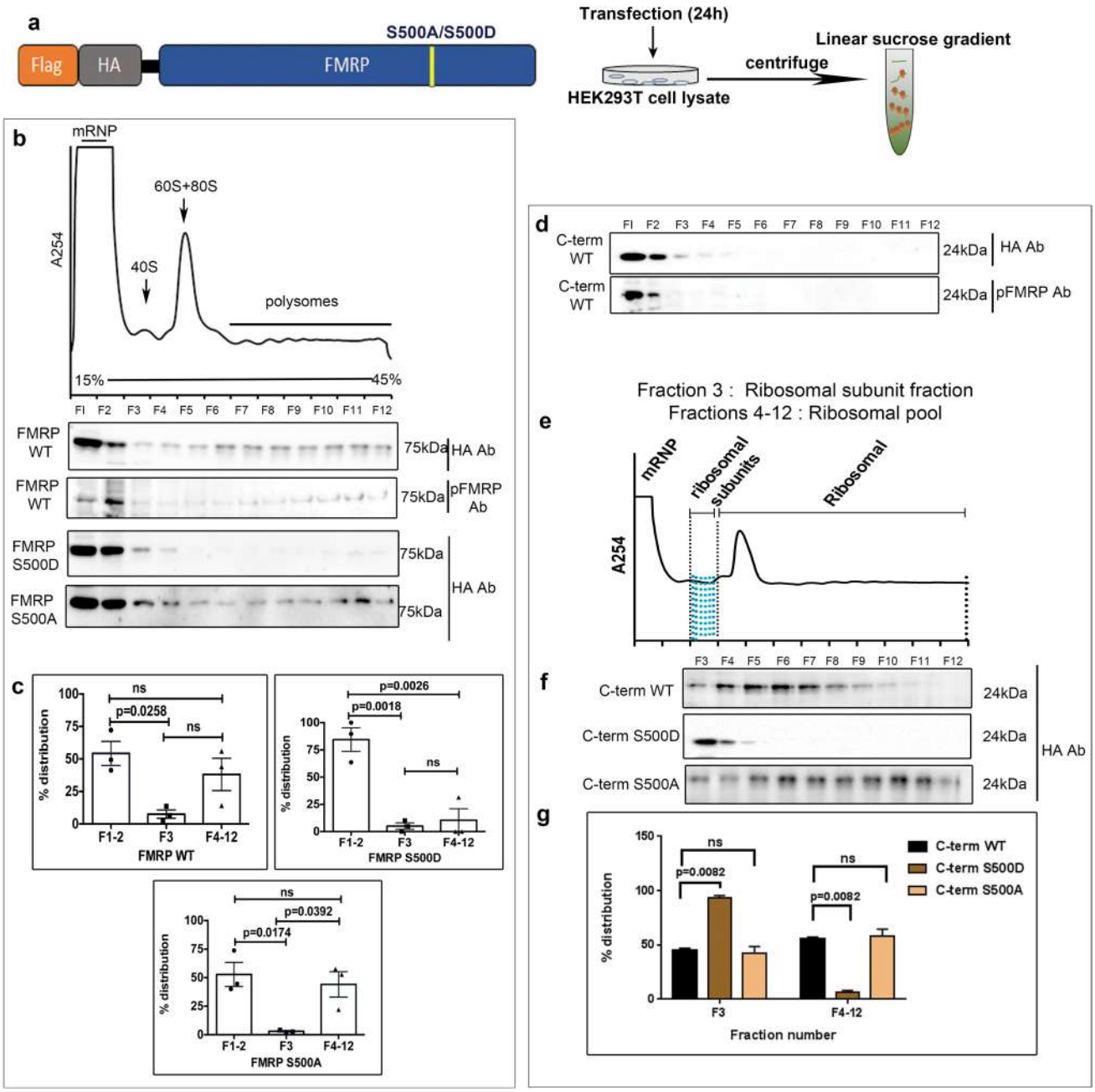

intensity on Y-axis for both untreated and puromycin treatment conditions. A regression analysis was performed for the same data to test the linear dependency of RPL10 and FMRP.

Statistical Analysis

All statistical analyses were performed using Graph Pad Prism software. The normality of the data was tested using the Kolmogorov–Smirnov test. For experiments with less than 5 data points, parametric statistical tests were applied [34]. Data were represented as mean ± SEM in all in vitro and polysome experiment graphs. FUNCAT and puncta data was represented as boxes and whiskers with all the individual data points. Statistical significance was calculated using unpaired Student's *t*-test (2 tailed with equal variance) in cases where 2 groups were being compared. One-way ANOVA was used for multiple group comparisons, followed by Tukey's multiple comparison tests, Bonferroni's multiple comparison test, or Dunnett's multiple comparison test. *P*-value less than 0.05 was considered to be statistically significant.

◂**Fig. 2** Phosphorylation of FMRP C-terminus determines its ribosome association. **a** Schematic describing FMRP WT, S500D, and S500A mutants of FMRP that were transfected in HEK293T cells for 24 h before subjecting it to polysome profiling on a linear sucrose gradient. **b** Top – representative polysome trace obtained at 254 nm indicating the division of fractions into mRNP, 40S, 60S + 80S, and polysomes. Bottom – representative immunoblots indicating the distribution of overexpressed full-length FMRP WT, FMRP S500D, and FMRP S500A along the 12 fractions of linear sucrose gradient. FMRP WT-transfected fractions were also probed for phospho FMRP with anti-pFMRP (Serine500) antibody ($n = 3$). **c** Top–graph indicating the quantification of overexpressed FMRP variants among the mRNP (F1-2), ribosomal subunits (F3), and ribosomal fractions (F4–12) $n = 3$. One-way ANOVA $p = 0.0291$ with Tukey's multiple comparison test for FMRP WT and $p = 0.0012$ with Tukey's multiple comparison test for FMRP S500D. Bottom–graph indicating the quantification of FMRP S500A among the mRNP (F1–2), ribosomal subunits (F3), and ribosomal fractions (F4–12) $n = 3$. One-way ANOVA $p = 0.0158$ with Tukey's multiple comparison test. **d** Representative immunoblots indicating the distribution of C-term WT overexpressed in HEK293T cells along the 12 fractions of the linear gradient. Fractions were also probed for phospho (at Serine500) C-term distribution with anti-pFMRP (Serine500) antibody ($n = 3$). **e** Representative polysome profile with trace obtained at 254 nm. Schematic indicates the division of fractions based on the presence of assembled ribosomal subunits. Fraction 3 corresponds to the ribosomal subunit pool. Fractions 4–12 correspond to the ribosomal pool. **f** Representative immunoblots indicating the distribution of overexpressed C-term WT, phosphomimetic (C-term S500D), and dephosphomimetic (Cterm-S500A) along fractions 3 to 12 of a linear sucrose gradient. Blots were probed with anti-HA antibody ($n = 3$). **g** Graph indicating the quantification of overexpressed C-term variants in ribosomal subunit fraction (F3) versus ribosomal fractions (F4–12). $n = 3$ for each condition. Data represented as mean ± SEM, one-way ANOVA $p = 0.004$ for F3, $p = 0.004$ for F4–12 followed by Bonferroni's multiple comparisons test

Results

C-terminus of FMRP is Responsible for Direct Binding to Ribosomes

FMRP is a modulator of activity-mediated translation in the nervous system [14, 35, 36] and an important requirement for this function is the ability of FMRP to interact with ribosomes and polysomes [37]. This feature was clearly shown in the *I304N* FMRP mutant, which does not associate with polysomes, but retains its RNA binding capacity [18]. FMRP is a multi-domain protein and it is important to understand which of these domains is essential for its interaction with ribosomes. We fragmented human FMRP into three parts, the N-terminus containing tudor domains (N-term), the KH1 and KH2 domains (collectively called the KH domain here), and the C-terminus containing the RGG box (C-term). To address the contribution of these domains of FMRP in ribosome association, first, we used HEK293T cell lysate. Recombinant proteins corresponding to N-term (1–216 aa), KH domains (217–425 aa), and C-term (426–632 aa) of FMRP (Fig. 1a) bearing N-terminal GST tag were expressed in *E. coli* Rosetta DE3 cells. We used a baculoviral-based SF9 insect cell system to express 6His-tagged full-length human FMRP (His-FMRP) since its expression in *E. coli* resulted in multiple truncated versions of the protein (Fig. 1a).

Purified His-FMRP (150 pmol) was spiked with the HEK293T lysate and subjected to polysome profiling. The distribution of ribosomes along the sucrose gradient was visualized through distribution of RPLP0 and RPS6 proteins, representing the large and small subunits of the ribosome respectively (Fig. 1b). A significant part of endogenous FMRP and His-FMRP co-fractionated with both ribosomal and polysomal fractions (Fig. 1b, c, e and S1h). To rule out a potential biochemical artifact from the spiked proteins, we also performed polysome profiling assays by over expressing Flag-HA FMRP in HEK293T cells (Fig S1a). Overexpressed Flag-HA FMRP was distributed across all fractions of the linear sucrose gradient similar to the spiked His-FMRP protein (Fig. S1b and S1d). A total of 150 pmol of each recombinant domain were spiked into HEK293T cell lysate followed by its separation on a 15–45% linear sucrose gradient. An antibody against the GST tag was used for the detection of all the spiked domain proteins. N-term and KH domains were present only in the non-ribosomal/mRNP fractions (fractions 1 and 2) where RPLP0 and RPS6 were absent (Fig. 1b, d, f, g). We obtained similar distribution with HEK293T cells transfected with Flag-HA N-term and Flag-HA KH constructs (Fig. S1c, S1e and S1f). This was quite unexpected since the KH domain has been previously reported to be important for polysome distribution of FMRP [18]. Additionally, there was no significant improvement in polysome association on fusing N-term to the KH domain (Fig. S1c and S1g). Importantly, only the C-terminus domain showed a similar polysome distribution of the full-length FMRP protein (Fig. 1d, h). Purified GST alone was spiked in HEK293T cell lysate as a control and it did not enter into either ribosomal or polysome fractions (Fig. 1i). Thus, our results suggest that the C-terminus domain of FMRP is important for its association with ribosomes/polysomes.

To further validate the minimal domain of FMRP involved in the interaction with ribosomes, we performed pull-down assays with recombinant FMRP domains mixed with HEK293T cell lysate or purified human 80S ribosomes (Fig. 1j). HEK293T cell lysates were spiked with 50 pmol of GST-tagged domains and incubated with glutathione beads. Elutes from the beads were assayed for the presence of 18S and 28S rRNA by qPCR (as a readout for ribosomes) (Fig. 1j). Our results clearly show that 18S and 28S rRNA were significantly pulled down only by C-term

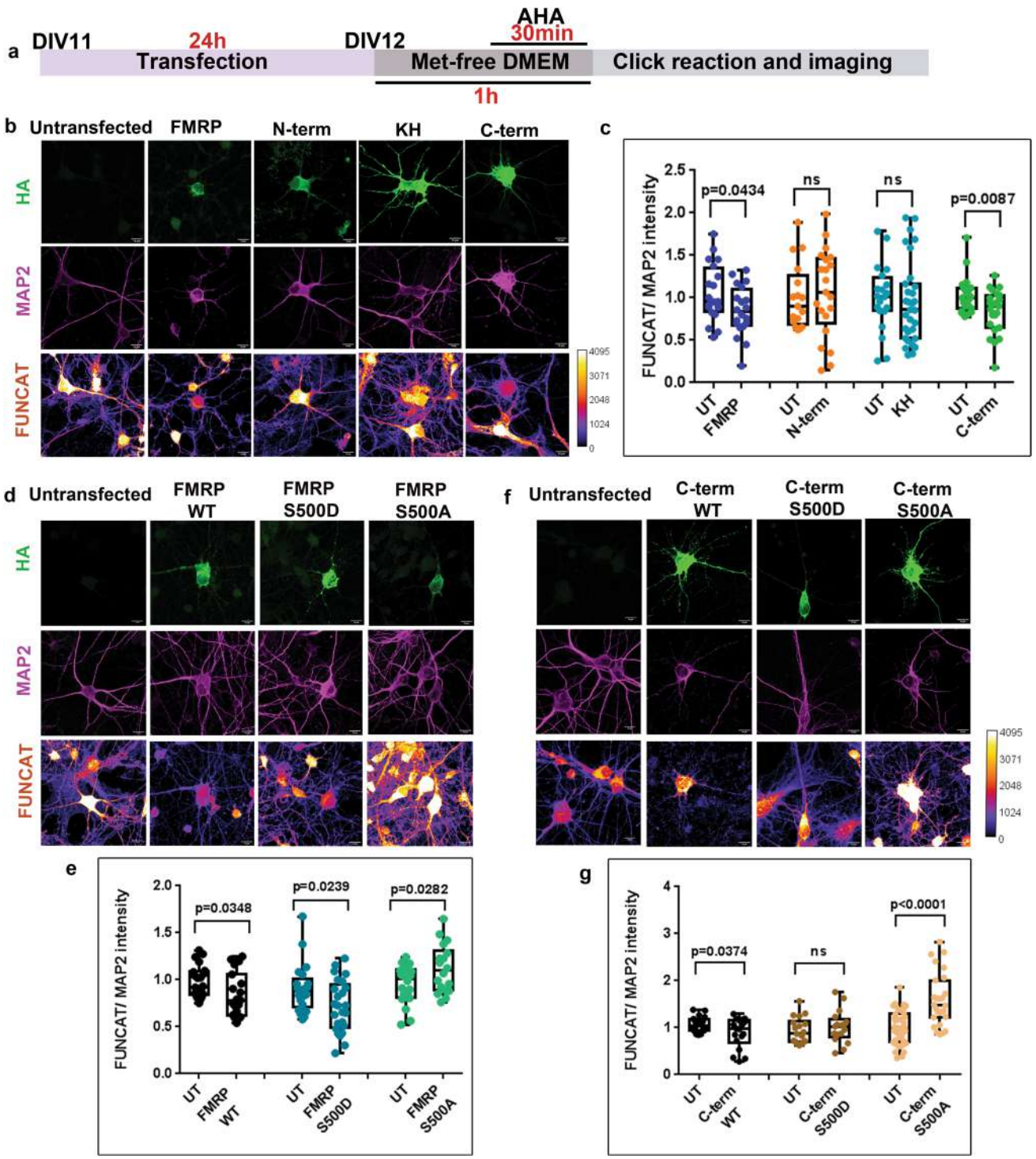

of FMRP (Fig. 1k, l). In contrast, GST-N-term and GST-KH did not show any significant pull down of 18S and 28S rRNA, similar to control GST (Fig. 1k, l). Alternatively, elutes were also assayed for the presence of RPS6 and RPLP0 ribosomal proteins. Once again, only C-term was associated with ribosomal proteins as compared to N-term, KH, and GST alone (Fig. 1m). We performed an in vitro binding assay with purified mRNA-free human 80S ribosomes and molar excess of GST-tagged domains (10×). Elutes were probed for the enrichment of 18S and 28S rRNA (Fig. 1n, o) as well as ribosomal proteins RPLP0 and RPS6 (Fig. 1p). Similar to the results with HEK293T lysates, we observed that only C-term of FMRP associated with purified 80S ribosomes.

◂**Fig. 3** C-terminus is responsible for FMRP-mediated translation regulation in neurons. **a** Experimental workflow. Primary rat cortical neurons (DIV11) were transfected for 24 h with full-length and FMRP domains. Transfected neurons were subjected to fluorescent non-canonical amino acid tagging (FUNCAT) along with immunostaining for HA and MAP2.**b** Representative images for HA, MAP2, and FUNCAT fluorescent signal in neurons transfected with full-length FMRP and FMRP domains (scale bar—10 µm). **c** Quantification of the FUNCAT fluorescent intensity normalized to MAP2 fluorescent intensity for full-length and domains of FMRP. For each FMRP construct, the FUNCAT signal from the transfected neuron was normalized to the untransfected neuron. Whiskers range from minimum to maximum data point. Unpaired *t*-test for each construct, $n = 15–30$ neurons from 5 independent experiments. **d** Representative images for HA, MAP2 and FUNCAT fluorescent signal in neurons transfected with full-length FMRP WT, S500D, and S500A variants (scale bar—10 µm).**e** Quantification of the FUNCAT fluorescent intensity normalized to MAP2 fluorescent intensity for full-length FMRP WT, S500D, and S500A. Unpaired *t*-test for each construct, $n = 20–40$ neurons from 4 independent experiments. **f** Representative images for HA, MAP2, and FUNCAT fluorescent signal in neurons transfected with C-terminus WT, S500D and S500A variants (Scale bar—10 µm).**g** Quantification of the FUNCAT fluorescent intensity normalized to MAP2 fluorescent intensity for C-terminus WT, S500D, and S500A variants. Unpaired *t*-test for each construct, $n = 20–40$ neurons from 4 independent experiments

Phosphorylation of FMRP C-term Determines its Ribosome Association

Post-translational modifications such as phosphorylation are known to modulate many functions of FMRP: RNA binding and protein–protein interactions in particular [20]. The primary site for phosphorylation is Serine 500 within the C-terminus domain of hFMRP [20, 22]. Hence, we postulated that altering the phosphorylation status of FMRP could alter its association with ribosomes/polysomes [22]. We transfected HEK293T cells with Flag-HA-tagged FMRP WT, phosphomimetic (FMRP S500D), and de-phosphomimetic (FMRP S500A) for 24 h followed by separation on a linear sucrose gradient (Fig. 2a). Under steady-state conditions, FMRP WT sediments with ribosomal (fractions 3–12 including subunits) as well as non-ribosomal fractions (fractions 1 and 2) (Fig. 2b, c). Immunoblots from the same fractions, probed with an antibody against phosphorylated Serine500 (p-FMRP), clearly showed an accumulation of phosphorylated FMRP only in the initial fractions (fractions 1–2) (Fig. 2b). Similarly, FMRP S500D was significantly present only in the non-ribosomal fractions (fractions 1–2) (Fig. 2b, c). FMRP S500A was distributed in all the fractions including polysomes (fractions 1–12), as observed with FMRP WT (Fig. 2b, c).

To test this at the level of domains, we transfected HEK293T cells with Flag-HA FMRP C-term and subjected it to polysome profiling. We observed that the C-term domain, which contains the primary phosphorylation site Serine 500, was mostly restricted to the initial fractions of the sucrose gradient (Fig. 2d). Probing the same fractions with a p-FMRP antibody showed that the initial fractions of the C-term domain were phosphorylated (Fig. 2d). We investigated if altering the phosphorylation of Serine 500 in C-term could improve its distribution in the polysomal fractions. To test this, we overexpressed the phosphomimetic (C-term S500D) and de-phosphomimetic (C-term S500A) in HEK293T cells and examined their polysome distribution (Fig. 2f, g). Since the over-expression of full-length FMRP, C-term, and their phosphomutants were performed in HEK293T cells in the background of endogenous FMRP, we suspected that there could be a modulation in the expression of our constructs and their association with ribosomes. Hence, to understand the difference in the distribution between C-term WT, C-term S500D, and C-term S500A, we quantified the amount of overexpressed protein in fraction 3 (ribosomal subunit) versus fractions 4–12 (ribosome + polysomes) (Fig. 2e). C-term S500A showed a significant increase in polysome association and conversely C-term S500D showed significant accumulation in the initial fractions (Fig. 2f, g). Together with our previous results, we conclude that C-term alone is sufficient to bind to the ribosome and this association is further enhanced through dephosphorylation (Fig. 2f, g).

Finally, we generated a combination of KH and C-term domains (referred to as KH + C-term) and investigated its polysomal distribution (Fig. S2a). We observed that most of the overexpressed KH + C-term was found to be in the initial fractions of the linear gradient (Fig. S2a). Immunoblotting with p-FMRP antibody showed that accumulated KH + C-term is phosphorylated (Fig. S2a). Similarly, the difference in ribosomal association between WT, S500D, and S500A mutants of KH + Cterm was distinguishable only when quantified between fractions 3 and fractions 4–12 (Fig S2b and S2c). We clearly observed that the dephosphorylation of KH + Cterm significantly increased its association with the heavier ribosomal fractions (Fig. S2c). This further confirms that the phosphorylation status of FMRP can indeed dictate its ribosome binding ability.

The C-terminus of FMRP Alone Is Sufficient to Inhibit Global Protein Synthesis in Neurons

FMRP is primarily described as a modulator of protein synthesis in neurons, which at basal level, is shown to induce translation inhibition [8, 14, 20, 38]. But the contribution of individual domains of FMRP in regulating translation is not known. To examine this, we transfected rat primary cortical neurons with Flag-HA-tagged N-term, KH, and C-term of FMRP and measured de novo protein synthesis through FUNCAT (fluorescent non-canonical amino-acid tagging) (Fig. 3a) [39]. As expected, there was a significant reduction in the FUNCAT signal on

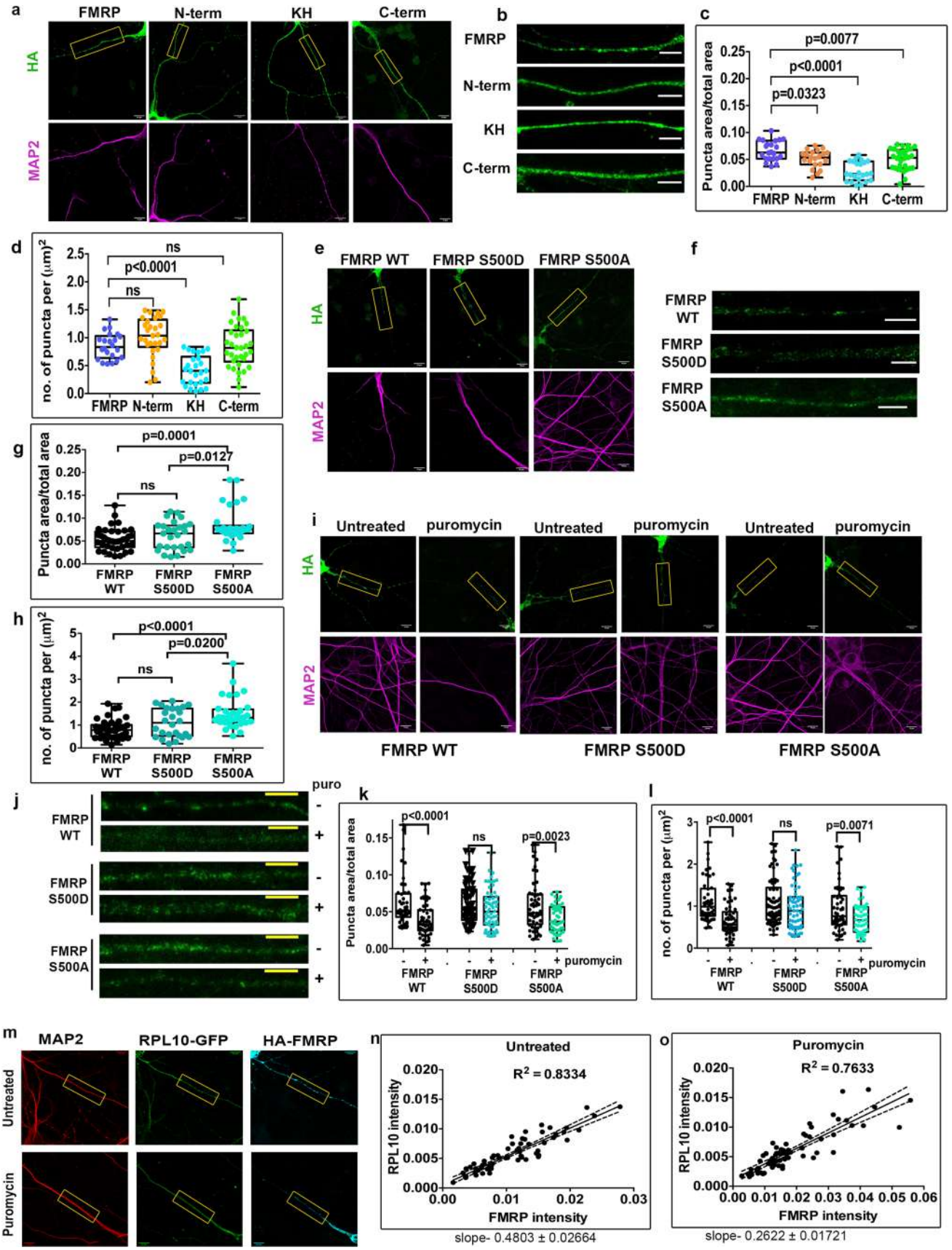
a
FMRP
N-term
KH
C-term
HA
MAP2
b
FMRP
N-term
KH
C-term
c
p=0.0077
p<0.0001
p=0.0323
Puncta area/total area
FMRP N-term KH C-term
d
ns
p<0.0001
ns
no. of puncta per (μm)²
FMRP N-term KH C-term
e
FMRP WT
FMRP S500D
FMRP S500A
HA
MAP2
f
FMRP WT
FMRP S500D
FMRP S500A
g
p=0.0001
p=0.0127
ns
Puncta area/total area
FMRP WT
FMRP S500D
FMRP S500A
h
p<0.0001
p=0.0200
ns
no. of puncta per (μm)²
FMRP WT
FMRP S500D
FMRP S500A
i
Untreated
puromycin
Untreated
puromycin
Untreated
puromycin
HA
MAP2
FMRP WT
FMRP S500D
FMRP S500A
j
puro
FMRP WT
FMRP S500D
FMRP S500A
k
p<0.0001
ns
p=0.0023
Puncta area/total area
puromycin
FMRP WT
FMRP S500D
FMRP S500A
l
p<0.0001
ns
p=0.0071
no. of puncta per (μm)²
puromycin
FMRP WT
FMRP S500D
FMRP S500A
m
MAP2
RPL10-GFP
HA-FMRP
Untreated
Puromycin
n
Untreated
R² = 0.8334
RPL10 intensity
FMRP intensity
slope- 0.4803 ± 0.02664
o
Puromycin
R² = 0.7633
RPL10 intensity
FMRP intensity
slope- 0.2622 ± 0.01721

◂**Fig. 4** FMRP puncta size is regulated by phosphorylation and puncta are puromycin sensitive. **a** HA and MAP2 fluorescent intensities in primary cortical neurons transfected with full-length FMRP and domains (scale bar—10 µm). **b** Enlarged inlets of panel **a** showing dendritic localization of puncta (scale bar—5 µm). **c** Puncta area by total dendritic area for full-length and domains of FMRP. One-way ANOVA $p<0.001$ with Tukey's multiple comparison's test $n=25$–35 neurons from 5 independent experiments. **d** Number of puncta per unit area of the dendrite for full-length and domains of FMRP. One-way ANOVA $p<0.001$ with Tukey's multiple comparison's test, $n=25$–35 neurons from 5 independent experiments. **e** HA and MAP2 fluorescent intensities in primary cortical neurons transfected with full-length FMRP WT, S500D, and S500A variants (scale bar—10 µm). **f** Enlarged inlets of **e** showing dendritic localization of puncta (scale bar—5 µm). **g** Puncta area by total dendritic area for full-length FMRP WT, S500D, and S500A. One-way ANOVA $p=0.0002$ with Tukey's multiple comparison test $n=20$–40 neurons from 5 independent experiments. **h** Number of puncta per unit area of the dendrite for full-length FMRP WT, S500D, and S500A. One-way ANOVA $p<0.0001$ with Tukey's multiple comparisons test. $n=25$–40 neurons from 5 independent experiments. **i** HA and MAP2 fluorescent intensities in primary cortical neurons transfected with full-length FMRP WT, S500D, and S500A followed by treatment with puromycin (1 mM) for 1 h (scale bar—10 µm).**j** Enlarged inlets of ***i*** showing dendritic localization of puncta (scale bar—5 µm). **k** Puncta area by total dendritic area for full-length FMRP WT, S500D, and S500A on Puromycin treatment. Unpaired *t*-test. $n=40$–60 neurons from 3 independent experiments. **l** Number of puncta per unit area of the dendrite for full-length FMRP WT, S500D, and S500A on puromycin treatment. Unpaired *t*-test. $n=40$–60 neurons from 3 independent experiments. **m** MAP2, HA, and GFP intensities in primary cortical neurons co-transfected with HA-FMRP and RPL10-GFP followed by puromycin treatment (1 mM) for 1 h (scale bar—10 µm). **n** Scatter plots indicating distribution of RPL10 intensity and FMRP intensity in FMRP puncta under basal conditions. Dots represent normalized mean intensities of RPL10 and FMRP. $n=67$ dendrites from 4 independent experiments. Slope $=0.4803\pm0.02664$. **o** Scatter plots indicating distribution of RPL10 intensity and FMRP intensity in FMRP puncta on puromycin treatment (1 mM for 1 h). Dots represent normalized mean intensities of RPL10 and FMRP. $n=74$ dendrites from 4 independent experiments. Slope $=0.2622\pm0.01721$

over-expression of full-length FMRP in comparison to the untransfected neurons (Fig. 3b, c). Interestingly, we found that C-term alone could significantly decrease the FUNCAT signal by 25% similar to full-length FMRP (Fig. 3b, c). Although KH domains have been previously shown to be indispensable for inhibition of target mRNA translation, we did not capture any significant change in the FUNCAT signal in KH-transfected neurons (Fig. 3b, c). Similarly, transfection of N-term alone also did not alter the FUNCAT signal demonstrating that N-term has no effect on global translation (Fig. 3b, c).

Previously we highlighted the role of phosphorylation in influencing FMRP-ribosome association (Fig. 2b). We tested if the phosphorylation status of FMRP can also influence global translation regulation. We transfected rat primary cortical neurons at DIV11 with FMRP WT, S500D and S500A constructs for 24 h prior to FUNCAT (Fig. 3d). As indicated in earlier results, over-expression of FMRP WT significantly reduced FUNCAT signal indicating an inhibition in total protein synthesis (Fig. 3d, e). Likewise, over-expression of phosphomimetic FMRP S500D also led to a reduction in the FUNCAT signal. On the contrary, FMRP S500A showed a significant increase in the FUNCAT signal in comparison to untransfected neurons (Fig. 3d, e). In a parallel experiment WT, S500D, and S500A mutants of C-term were transfected in neurons to determine if C-term also follows a similar mechanism in regulating translation. We captured a similar reduction in FUNCAT signal with over-expression of C-term WT and a consistent increase in FUNCAT signal with C-term S500A mutant (Fig. 3f, g). However, the FUNCAT signal in the neurons transfected with C-term S500D was unchanged (Fig. 3f, g). Taken together, our results conclude that the C-term of FMRP is the primary driver of translation regulation and C-term alone can capture the translation switch of FMRP by modulating its phosphorylation status.

FMRP Puncta Size is Regulated by Phosphorylation and Puncta are Sensitive to Puromycin

FMRP has been shown to be a component of dynamic membrane-less granules in neurons [16, 40, 41]. This process of granule formation is shown to be induced by phase separation of the intrinsically disordered region (IDR) of FMRP in vitro [40]. However, the role of other domains in formation of granules in mammalian cells is unclear. To investigate this, we over-expressed Flag-HA-tagged domains of FMRP in rat primary cortical neurons and quantified the size and relative number of the neuronal puncta containing these tagged proteins (Fig. 4a, b). We observed that the puncta of all individual domains of FMRP were smaller in area compared to that of full-length FMRP (Fig. 4c). However, KH domain containing puncta were the least in number in comparison to the full-length protein (Fig. 4d). His-GFP, which was transfected as a control, showed a diffuse pattern of expression (non punctate) compared to the punctate expression of FMRP (Fig. S3a, S3b and S3c). Interestingly, puncta containing KH domain was not significantly different from that of GFP-containing puncta, indicating that KH domain alone has the least puncta-forming ability among other domains of FMRP (Fig. S3a, S3b and S3c). On fusing KH to either the N-term or C-term, we observed an increase in puncta size and puncta number, although they were not as good as the full-length protein (Fig. S3d, S3e and S3f).

To investigate the role of phosphorylation in puncta formation, we transfected FMRP WT, FMRP S500D and FMRP S500A in rat primary cortical neurons and examined changes in puncta characteristics in neurons (Fig. 4e, f). Interestingly, over-expression of FMRP S500A resulted in a significant increase in puncta area (Fig. 4g). We also observed a significant increase in the number of puncta in neurons transfected with FMRP S500A (Fig. 4h). FMRP S500D containing puncta were similar in size and number to puncta containing FMPR WT (Fig. 4g, h). This result indicates that dephosphorylation of FMRP has

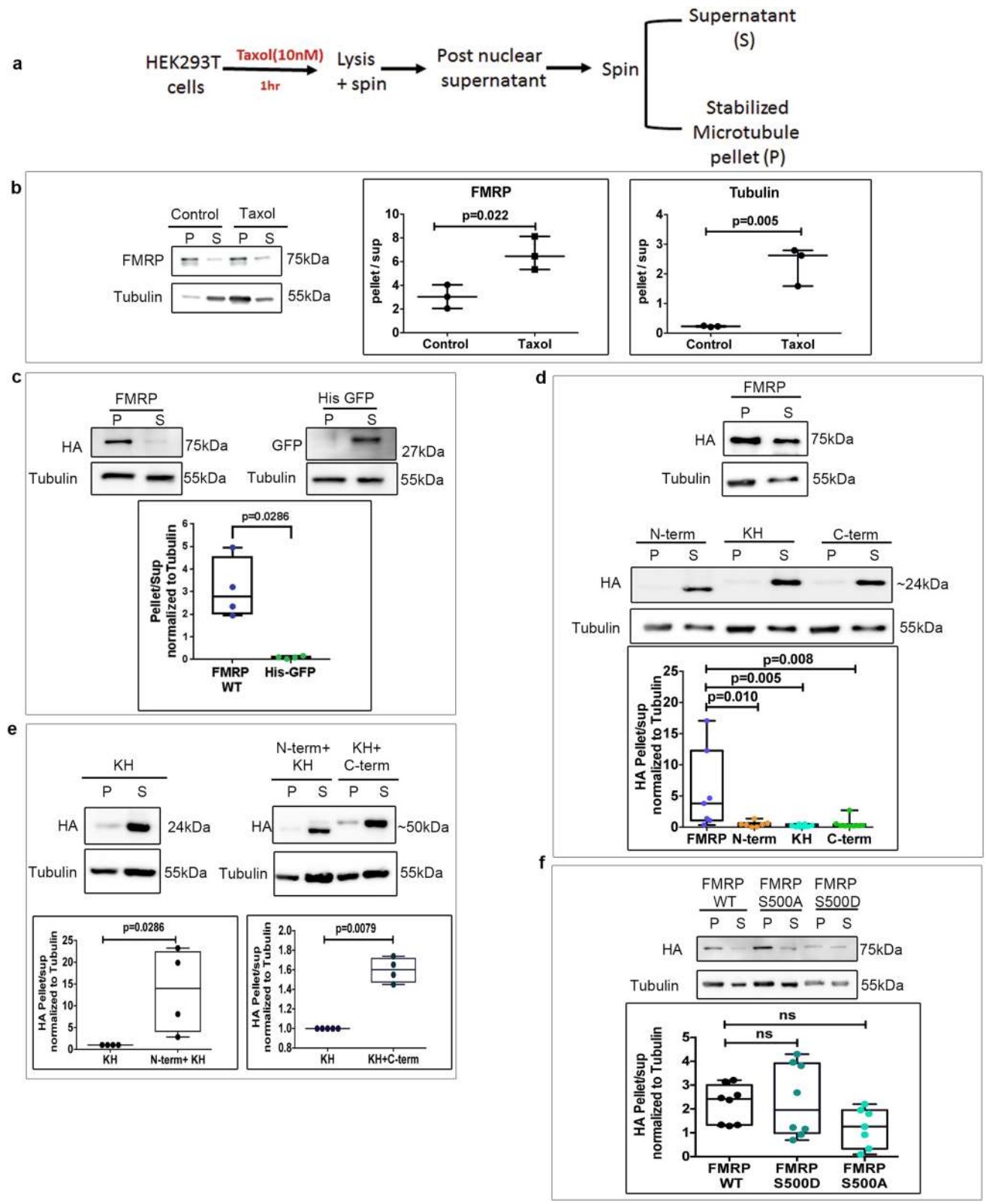

a significant influence on the size and number of FMRP-containing puncta. Interestingly, this did not apply to overexpressed WT, S500D, and S500A mutants of C-term and KH + C-term domains (Fig. S3g-h and S3k-l). Altering the phosphorylation status of either C-term alone or KH + C-term did not affect the size or number of the puncta (Fig. S3i-j and S3m-n).

◂**Fig. 5** KH domain of FMRP is necessary but not sufficient enough for FMRP-Microtubule association. **a** Schematic for microtubule enrichment assay on Taxol (10 nM) treatment. **b** Left– Immunoblots indicating the enrichment of endogenous FMRP and tubulin in microtubule pellet on Taxol treatment in HEK293T cells. Middle – ratio of FMRP enrichment in pellet/supernatant on DMSO (control) and Taxol treatment. Right – ratio of tubulin enrichment in pellet/supernatant on DMSO (control) and Taxol treatment. Data represented as mean ± SEM, unpaired *t*-test ($n=3$). **c** Top – immunoblots indicating enrichment of WT FMRP in microtubule pellet and His-GFP in the supernatant on Taxol treatment. Bottom – box plot indicating the ratio of FMRP and His-GFP enrichment in pellet/supernatant on Taxol treatment. Unpaired *t*-test ($n=4$). **d** Immunoblots of HEK293T cell microtubule pellet enriched on Taxol treatment after transfection with full-length and FMRP domains. Box plots represent the pellet/ supernatant ratio. One-way ANOVA $p=0.0053$ followed by Dunnett's multiple comparisons test ($n=7$–8). **e** Immunoblots of HEK293T cell microtubule pellet enriched on Taxol treatment after transfection with KH, N-term + KH, and KH + C-term. Box plots represent the pellet/supernatant ratio. Unpaired *t*-test ($n=4$–5). **f** Immunoblots of HEK293T cell microtubule pellet enriched on Taxol treatment after transfection with FMRP WT, FMRP S500D, and FMRP S500A. Box plots represent the pellet/supernatant ratio. One-way ANOVA $p=0.1325$ followed by Dunnett's multiple comparisons test ($n=7$–8)

The molecular constituents of FMRP granules are still unknown. It is unclear if FMRP is incorporated into translating ribosomes within these granules. To determine the translational status of FMRP-containing granules, we transfected neurons with FMRP WT, S500D, and S500A and analyzed the characteristics of the puncta after treatment with protein synthesis inhibitor Puromycin (Fig. 4i, j). Puromycin treatment leads to the dissociation of actively translating ribosomes/polysomes thus inhibiting protein synthesis. Interestingly, on Puromycin treatment, we observed a significant drop in the number and size of FMRP WT puncta (Fig. 4k, l). We also observed a similar reduction in size and number of FMRP S500A puncta indicating that these puncta contain actively translating ribosomes (Fig. 4k, l). FMRP S500D puncta were insensitive to Puromycin suggesting it to be consisting of stalled ribosomes (Fig. 4k, l). To further validate if FMRP-positive granules indeed contained actively translating ribosomes, we overexpressed RPL10-GFP (protein of the larger ribosomal subunit) along with FMRP WT and measured their colocalization after Puromycin treatment (Fig. 4m). Our data indicates that FMRP intensities in the puncta also correlate with RPL10 intensities directly demonstrating that ribosomal machinery co-localize to FMRP granules (Fig. 4n). The correlation between FMRP and RPL10 in FMRP puncta reduces on Puromycin treatment indicating that FMRP granules contain actively translating ribosomes (Fig. 4o). Together, our data demonstrates that each domain of FMRP is necessary in the formation of completely functional neuronal granules and phosphorylation modulates the characteristics of these FMRP-containing granules.

The KH Domain of FMRP Is Necessary but not Sufficient for FMRP-Microtubule Association

The absence of FMRP-regulated local translation in response to synaptic activity is a major underlying mechanism for cognitive impairment in FXS [13, 35, 36]. FMRP is shown to regulate the translation of a set of mRNAs in neurons through targeted localization in a microtubule-dependent manner [16]. To understand this biochemical interaction of FMRP with microtubules, we employed a previously described method to stabilize and extract microtubules and its interacting molecular partners using the drug paclitaxel/ Taxol (Fig. 5a) [37]. In this assay, we observed a significant amount of endogenous FMRP present in the microtubule pellet that got further enriched on treatment with Taxol, along with tubulin (Fig. 5b). Further on disrupting the microtubule network with nocodazole, we observed a depletion of both tubulin and FMRP in the pellet (Fig. S4a), confirming that the enrichment was microtubule specific. His-GFP was used as a negative control and it did not show any significant enrichment with microtubules on Taxol treatment (Fig. 5c).

Previously, it has been shown that the interaction of FMRP with microtubules is RNA-dependent [37]. To investigate this, we treated HEK293T cell lysate with RNase and observed a loss of FMRP from the microtubule-enriched pellet, confirming that FMRP-microtubule interaction is RNA-dependent (Fig S4b). To dissect out the contribution of the domains of FMRP in this interaction, HEK293T cells were transfected with N-term, KH, and C-term of FMRP followed by microtubule enrichment. Surprisingly, microtubule binding of all the individual domains of FMRP was significantly lower than that of the full-length FMRP protein (Fig. 5d). Next, we used N-term + KH and KH + C-term constructs in our microtubule-enrichment assay and observed that the combinations of domains significantly improved microtubule binding (Fig. 5e). The role of phosphorylation in FMRP-microtubule association has been poorly studied. To investigate this, we performed microtubule-enrichment assays with HEK293T cells transfected with FMRP WT, S500D and S500A constructs. Interestingly, neither of the phosphomutants showed any significant difference in comparison to FMRP WT with respect to microtubule association implying that this post-translational modification does not influence microtubule binding (Fig. 5f).

Single Nucleotide Mutations from Patients Reveal Functional Hierarchy in FMRP Domains

Fragile X syndrome (FXS) results from the silencing of the *FMR1* gene due to the expansion of an unstable triplet CGG motif present in the 5′UTR [42]. Nonetheless, high throughput sequencing studies have also revealed the presence of multiple single-point mutations that render

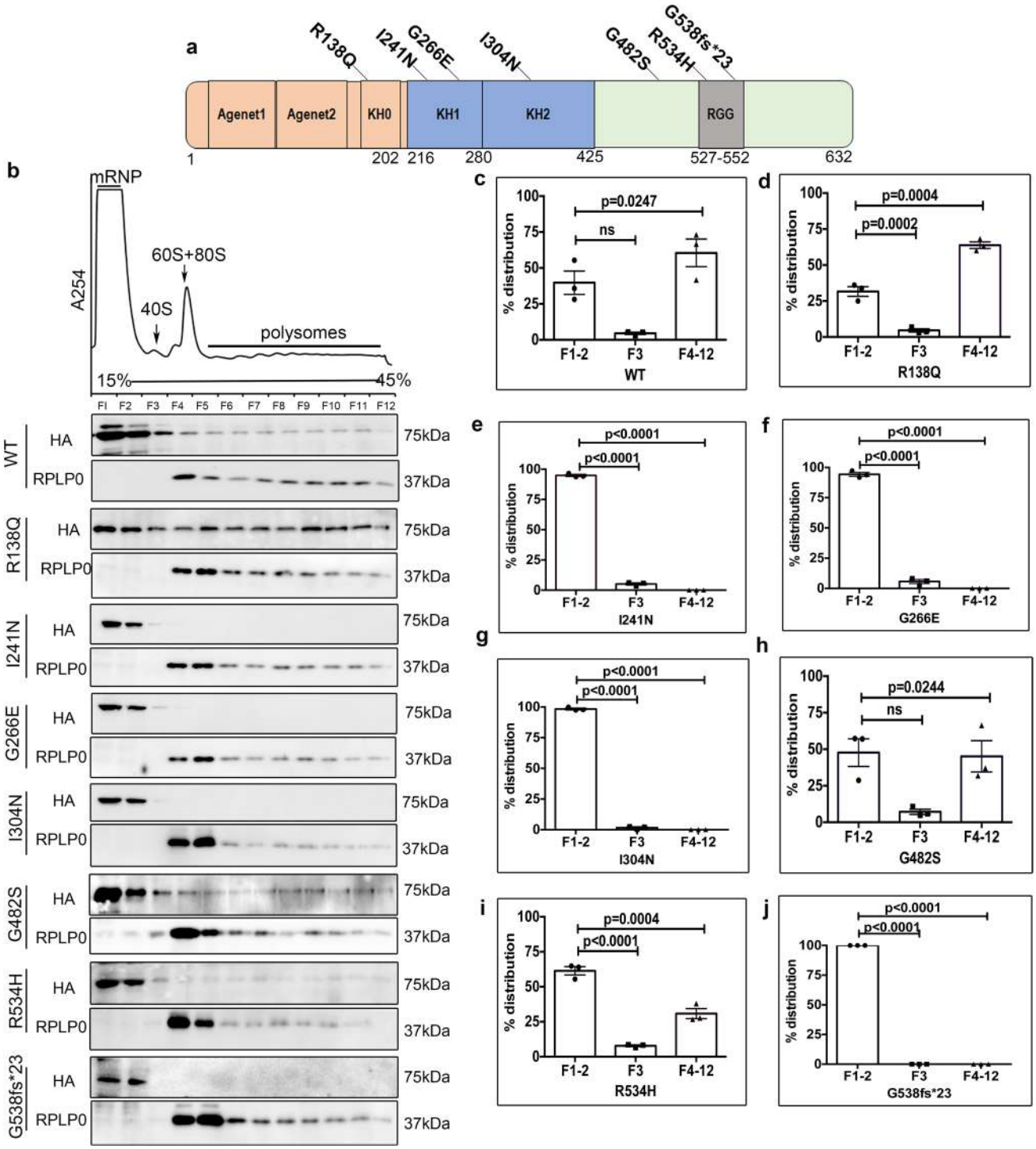

FMRP non-functional [30–32]. We made use of relevant pathogenic mutations in the N-term (*R138Q*), KH domains (*I304N, G266E*), and C-term (*G482S, R534H, G538fs*23*) of FMRP to understand the contribution of individual domains in its function [29–32]. We sought to investigate the impact of these mutations on the role of FMRP as a translation regulator. We generated Flag-HA FMRP constructs bearing selected single-point mutations in their respective domains (Fig. 6a). Additionally, we also generated a functionally relevant mutation in the KH1 domain (*I241N*) to mimic the well-studied patient identified mutation *I304N* that is present in the KH2 domain (Fig. 6a) [17]. First, we tested the impact of these mutations in ribosome association through linear sucrose density centrifugation (Fig. S5d). We observed that *I241N, I304N* and *G266E* mutations, residing in the KH

◂**Fig. 6** KH domain mutations drastically alter FMRP's association with ribosomes. **a** Schematic depicting position of mutations in FMRP identified in patients with FXS and intellectual disability. **b** Top – representative polysome trace of HEK293T cell lysate transfected with full-length FMRP WT and mutants for 24 h. Bottom – representative immunoblots indicating the distribution of FMRP mutants (probed with HA antibody) with corresponding distribution of ribosome fractions (probed with RPLP0 antibody). **c** Graph indicating the quantification of FMRP WT among the mRNP (F1–2), ribosomal subunits (F3), and ribosomal fractions (F4–12). $n=3$, one-way ANOVA $p=0.0045$ with Dunnett's multiple comparison test. **d** Graph indicating the quantification of FMRP R138Q among the mRNP (F1–2), ribosomal subunits (F3), and ribosomal fractions (F4–12). $n=3$, one-way ANOVA $p<0.0001$ with Dunnett's multiple comparison test. **e** Graph indicating the quantification of FMRP I241N among the mRNP (F1–2), ribosomal subunits (F3), and ribosomal fractions (F4–12). $n=3$, one-way ANOVA $p<0.0001$ with Dunnett's multiple comparison test. **f** Graph indicating the quantification of FMRP G266E among the mRNP (F1–2), ribosomal subunits (F3) and ribosomal fractions (F4–12). $n=3$, One-Way ANOVA $p<0.0001$ with Dunnett's multiple comparison test. **g** Graph indicating the quantification of FMRP I304N among the mRNP (F1–2), ribosomal subunits (F3), and ribosomal fractions (F4–12). $n=3$, one-way ANOVA $p<0.0001$ with Dunnett's multiple comparison test. **h** Graph indicating the quantification of FMRP G482S among the mRNP (F1–2), ribosomal subunits (F3), and ribosomal fractions (F4–12). $n=3$, one-way ANOVA $p=0.0238$ with Dunnett's multiple comparison test. **i** Graph indicating the quantification of FMRP R534H among the mRNP (F1–2), ribosomal subunits (F3), and ribosomal fractions (F4–12). $n=3$, one-way ANOVA $p<0.0001$ with Dunnett's multiple comparison test. **j** Graph indicating the quantification of FMRP G538fs*23 among the mRNP (F1–2), ribosomal subunits (F3), and ribosomal fractions (F4–12). $n=3$, one-way ANOVA $p<0.0001$ with Dunnett's multiple comparison test

domains of FMRP, drastically reduced its association with ribosomes and heavy polysomes presumably by affecting the RNA binding capacity of the protein (Fig. 6b, e-g). *R138Q* mutation in FMRP structurally preserves all the RNA binding domains and hence did not show any difference in polysome distribution in comparison to the WT protein as previously described (Fig. 6b–d) [2]. Similarly the C-term mutations *R534H* and *G482S* showed no change in polysome distribution in comparison to FMRP WT (Fig. 6b, i). *G538fs*23* mutation disrupts the RGG domain and generates an additional 23 novel amino acids in the C-term. This alteration of the C-term resulted in loss of ribosome/polysome binding (Fig. 6b, j).

Next, we sought to validate the functional effect of these mutations on translation regulation. Rat primary cortical neurons were transfected with Flag-HA FMRP mutants for 24 h and changes in global protein synthesis was assayed using FUNCAT. As shown previously, FMRP WT transfected neurons showed an overall reduction in the FUNCAT signal (Fig. 7a, b). This is in agreement with the general role of FMRP as an inhibitor of translation (Fig. 3b–e). On the contrary, while the KH domain mutations *I241N*, *G266E*, and *I304N* failed to inhibit translation, they also caused a significant increase in FUNCAT signal in comparison to untransfected neurons (Fig. 7a, b). Neurons transfected with the C-term mutants *G482S* and *R534H* did not exhibit any change in overall FUNCAT signal in comparison to respective untransfected neurons indicating that these mutations abolish the translation inhibitory function of FMRP (Fig. 7a, b). The C-term *G538fs*23* mutant also showed an increase in FUNCAT signal in the respective neurons (Fig. 7a, b). This gain-of-function could be attributed to the insertion of novel amino acid sequences within the C-term. Although our initial data indicated that *R138Q* mutation does not affect ribosome binding, we observed an increase in FUNCAT signal in comparison to untransfected neurons (Fig. 7a, b). Hence, we postulate that mutations might alter the characteristics of their respective domains thereby resulting in differential regulation of global translation.

Further, we sought to examine the effect of these mutations on microtubule binding. We transfected HEK293T cells with Flag-HA FMRP mutants and followed it by a microtubule enrichment assay. KH domain mutations such as *I241N*, *G266E*, and *I304N* did not get significantly enriched in the microtubule pellet in comparison to FMRP WT (Fig. 7c, d). Similarly C-term mutations *R534H* and *G538fs*23* also significantly hampered FMRP's association with microtubules compared to FMRP WT (Fig. 7c, d). However, we did not observe any significant effect of *R138Q* and *G482S* on FMRP-microtubule association (Fig. 7c, d). Together, our data concludes that distinct domains contribute to the precise functioning of FMRP in processes leading to translation regulation. Further, pathogenic mutations identified in the individual domains of FMRP affect their ability to associate with and regulate various components of translation.

Discussion

Here, we investigate the contribution of individual domains of FMRP in its primary role of translation regulation. On dissecting FMRP into single domains and domain combinations, we elucidate the independent and collective roles of the N-terminus, KH, and C-terminus domains in the processes of granule formation, microtubule binding and ribosome association. Our in vitro experiments and overexpression studies led us to an important conclusion that the C-terminus domain of FMRP is extremely essential for its binding to the ribosome. To this extent we also observe that the C-terminus domain alone is sufficient to inhibit protein synthesis in a manner similar to that of the full-length FMRP. An important feature of our study is that we were able to capture the dual role of FMRP as an activator and inhibitor of protein synthesis and this was primarily guided by its phosphorylation status. We show that phosphorylation is a principal post-translational modification (PTM) of

FMRP that acts as a molecular switch to regulate majority of its functions. Evidently there also exists a portion of FMRP that is not associated with translating polysomes. Our study also focuses on the alternate aspect of translation regulation whereby FMRP gets sequestered into mRNP containing granules that associate with microtubules. Unlike ribosome binding, our results reveal that single domains of FMRP cannot sufficiently mediate puncta formation and microtubule association. But in fact it requires the synergistic contribution from multiple individual domains to perform these functions efficiently.

FMRP has been proposed to regulate the translation of a large set of dendritic mRNAs [8, 43, 44]. Alternatively, FMRP is also known to globally inhibit protein synthesis in neurons [28]. The molecular mechanism underlying FMRP-mediated translation of these subsets of mRNA has been thoroughly studied [1, 8]. But we focused on understanding the mechanism of FMRP-mediated translation independent of sequence or structural features of the mRNA. It also directed our attention to determine which of the domains of FMRP are implicated in this process. Previously it was shown that hFMRP inhibits translation through direct binding of the C-terminus RGG domain to the ribosome [26]. Likewise, our in vitro binding assays indicate that the C-terminus domain alone can interact with the 80S ribosome while the N-terminus and KH domains cannot (Fig. 8a, b). A critical finding was that the C-terminus domain alone was sufficient enough to display ribosomal and polysomal association akin to that of the full-length FMRP.

Our primary observation is that FMRP co-fractionates with ribosomal as well as non-ribosomal fractions (including mRNPs). This direct binding to the ribosome blocks the binding of essential translational machinery, facilitating the inhibition of translation [45]. Our results describe an overall inhibition of protein synthesis in neurons expressing full-length FMRP. Independent studies separately claim that the KH and C-terminus domains are involved in this FMRP-mediated translation inhibition [26, 45] but our experimental observations support the C-terminus in translational inhibition, analogous to the full-length FMRP (Fig. 8a).

It is noteworthy that FMRP exists as a mixture of both phosphorylated and dephosphorylated forms in cells and phosphorylation is shown to influence the translation state of FMRP-associated ribosomes/polysomes [20, 21]. Through polysome profiling, we observe that phosphorylated FMRP gets enriched in the initial fractions of the gradient. Hence phosphorylation seems to redistribute FMRP into repressive granules. Stimulation of Gp1 mGluRs is shown to rapidly cause dephosphorylation of FMRP, a key feature in activity-mediated protein synthesis [20, 21]. Correspondingly, our study describes a key role for phosphorylation as a translational switch and how FMRP dephosphorylation (FMRP S500A) can activate protein synthesis by presumably increasing its ribosome association. As an alternate hypothesis, our observations of accumulated phospho-FMRP in the initial fractions of the linear sucrose gradient can indicate an inhibition in the elongation step of translation. On dephosphorylation of FMRP, this inhibition is lost, leading to the assembly of more ribosomes on mRNA and activation of translation. Our findings also emphasize that a similar mechanism of translation regulation exists between dephosphorylated forms of FMRP and C-term, where both increase translation (FMRP S500A and C-term S500A) (Fig. 8a). However, we could not capture the same molecular behavior between the phosphorylated forms of FMRP and C-term (FMRP S500D and C-term S500D).

In neurons, FMRP regulates dendritic mRNA translation to maintain multiple forms of plasticity [13, 14]. FMRP-bound target mRNA are shown to phase-separate into membrane-less granules in the cytoplasm and this is shown to be transported in a microtubule-dependent manner [40, 41]. The C-terminus has been extensively shown to drive FMRP granules/ puncta formation in vitro [40]. Despite these observations, the role of FMRP's domains in granule formation and cytoskeleton-mediated transport is still unknown. Our data shows that the individual domains of FMRP are incapable of forming neuronal puncta on their own. Correspondingly, neither of the individual domains could single-handedly contribute to FMRP-microtubule interaction. Formation of mRNP granules and their consequent dendritic transport is mediated through a combination of protein–protein as well as protein-RNA interactions. Hence, we speculate that the combination of domains improves microtubule association as well as puncta formation in comparison to their respective single domains (Fig. 8b).

Neuronal granules have been previously shown to contain components of translation machinery like ribosomes [16]. However the translation status of ribosomes within these granules is unknown. As shown previously, it is evident that phosphorylation of FMRP induces inhibition of translation (Fig. 3f). Also, phosphorylation is shown to increase FMRP's phase separation propensity while dephosphorylation favors granule disassembly [40]. We show that FMRP exists in phosphorylated and dephosphorylated states within granules and the area of the granules are dictated by the extent of phosphorylation. Additionally, our initial results postulate that phosphorylation might also influence the extent of ribosome binding within these granules. Inhibition of translation with Puromycin showed a striking reduction in the area and number of FMRP-containing granules and an even larger reduction with granules containing dephosphorylated FMRP. In addition, we also observe a reduction in the correlation between FMRP and ribosomes within FMRP-positive granules on inhibiting translation. This suggests that a majority of granules containing FMRP also contain

ribosomes, which are in an active state of translation elongation. FMRP-mediated local protein synthesis dictates that selected mRNA are stored in a repressed state with stalled polysomes within granules [46]. Following an appropriate signal, this repression is immediately relieved to provide the bulk of locally required proteins. Our data offers support to a

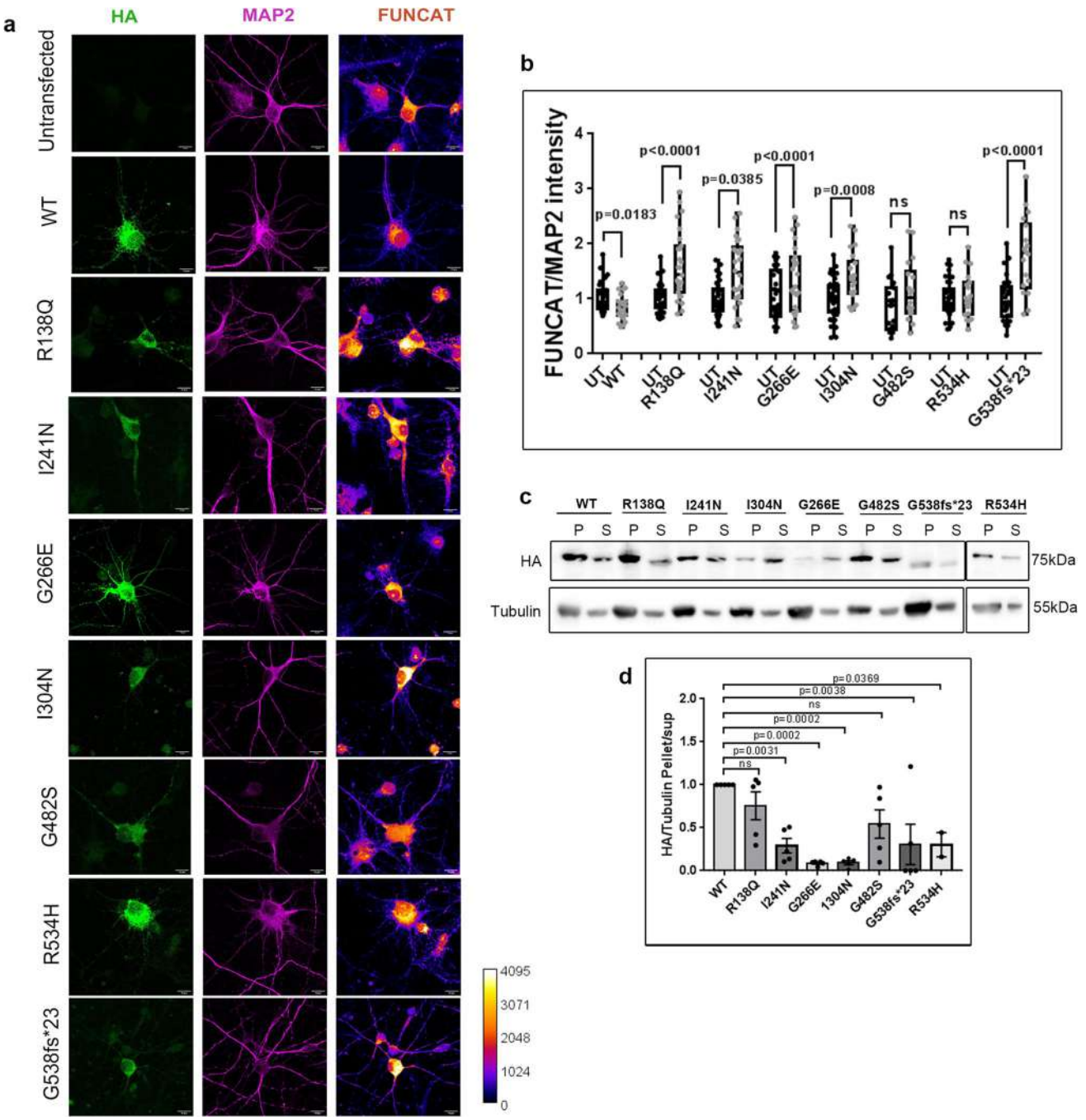

Fig. 7 KH domain mutations drastically alter FMRP's effect on translation and microtubule association. **a** Representative images for HA, MAP2, and FUNCAT fluorescent intensities in neurons transfected with full-length WT and FMRP mutants (Scale bar—10 µM). **b** Box plot representing the quantification of the FUNCAT fluorescent intensity normalized to MAP2 fluorescent intensity for WT and mutants of FMRP. For each FMRP construct, the FUNCAT signal from the transfected neuron was normalized to the untransfected neuron. Unpaired *t*-test, $n = 20–35$ neurons from 6 independent experiments. **c** Representative immunoblots indicating the enrichment of overexpressed WT FMRP, FMRP mutants, and tubulin in microtubule pellet and supernatant on Taxol treatment in HEK293T cells. ($n = 3–5$). **d** Bar graph indicating the ratio of enrichment of WT and FMRP mutants in pellet/supernatant on Taxol treatment of HEK293T. One-way ANOVA $p = 0.0002$, followed by Dunnett's multiple comparisons test ($n = 3–5$)

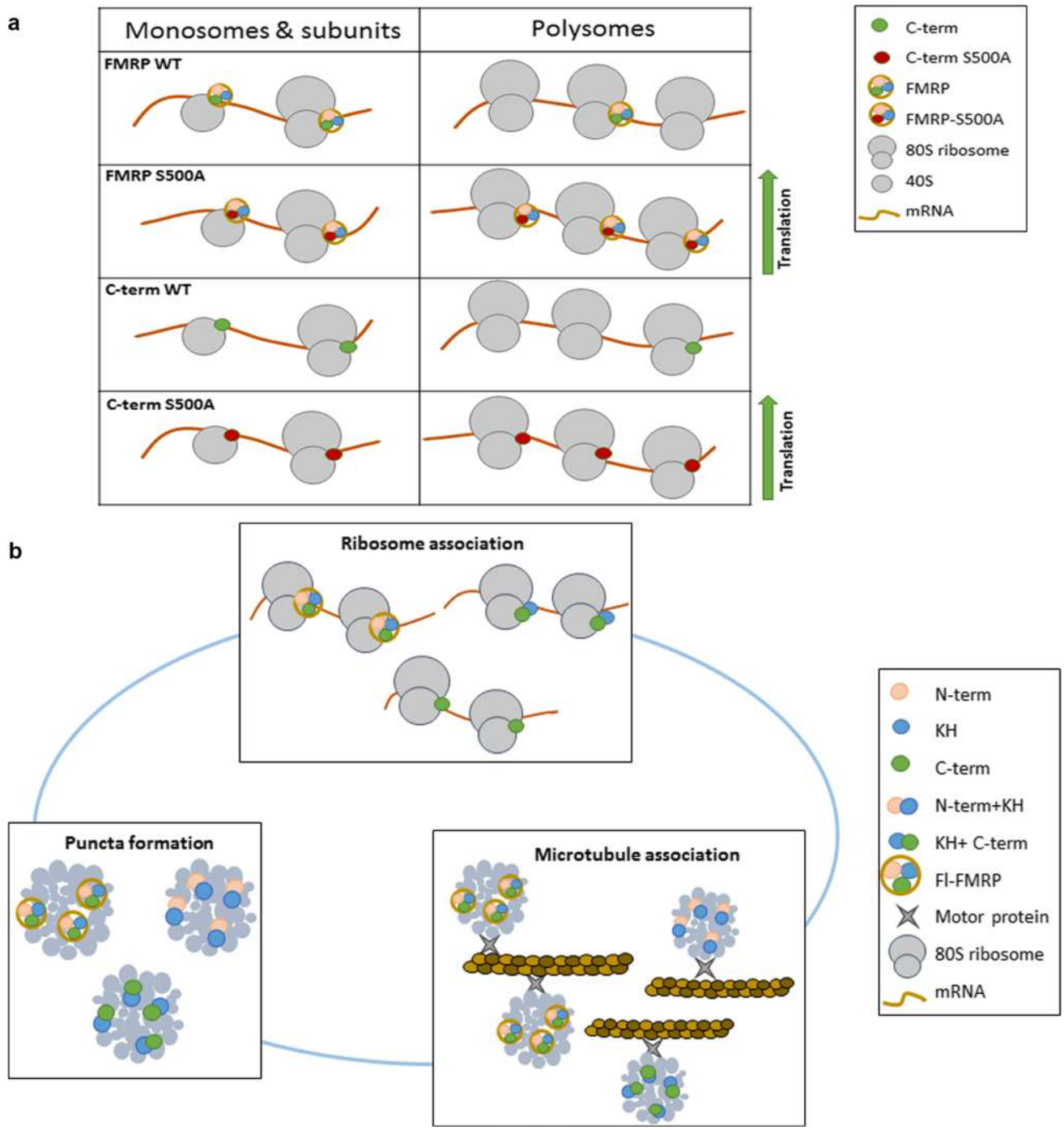

Fig. 8 **a** Model indicating that the C-terminus is sufficient to regulate the translation function of FMRP in neurons. This function is further regulated through the dephosphosphorylation of FMRP, which increases translation through increased association with ribosomes. **b** Model summarizing the minimal domains of FMRP required for puncta formation, microtubule association and association with ribosomes

contrasting hypothesis whereby mRNA can also be actively translated when accumulated within granules [47].

The canonical mutation leading to FXS is the CGG-repeat expansion in the 5′UTR of the *FMR1* gene. But several sequence variants of FMR1 have also been shown to cause FXS-like symptoms [30–32, 48, 49]. While most of these mutations have pathophysiological consequences, the molecular functions affected by them are unexplored. Through the use of point mutations, our study describes a hierarchical role of domains in cellular pathways that govern translation**.** Our results

show that the C-terminus domain is important for ribosome association and mutations in the C-terminus domain (*G482S* and *R534H*) generate loss-of-function FMRP variants incapable of inhibiting translation. The other C-terminus frame-shift mutation we investigated *G538fs*23* depicted increased translation, which may be due to the altered amino acid sequence. FMRP with N-terminus (*R138Q*) and KH domain mutations (*I241N*, *1304 N*, and *G266E*) also resulted in loss-of-function variants with respect to translation, although their C-terminus domain was unaffected. While the N-terminus and KH domain mutants failed to inhibit translation, they conversely increased global protein synthesis. This alternate mechanism of translation regulation adopted by the N-terminus and KH mutants is yet to be explored. The N terminus (*R138Q*) and KH mutant (*G266E*) proteins also fail to associate with microtubules, a function which likely precedes ribosome binding. Microtubule association comprises both RNA and protein interactions and the mutations could disrupt these properties, thus abolishing microtubule binding [29]**.** In conclusion, distinct domains of FMRP contribute to independent roles in translation regulation. The mutations in the domains account for its inadequate performance in specific molecular functions, thus indicating a strong hierarchical role of FMRP domains.

Abbreviations *FMRP*: Fragile X mental retardation protein; *RBP*: RNA binding protein; *RPS6*: Ribosomal protein S6; *RPLP0*: Ribosomal protein P0; *RPL10*: Ribosomal protein L10; *NMDAR*: N-methyl-D-aspartate receptor; *mGluR*: Metabotropic glutamate receptor; *FXS*: Fragile X Syndrome; *SNP*: Single nucleotide polymorphism; *FUNCAT*: Fluorescent non-canonical amino-acid tagging; *NLS*: Nuclear localization Signal; *DMSO*: Di-methyl sulphoxide; *ANOVA*: Analysis of variance; *E.coli*: Escherichia coli; *rRNA*: Ribosomal RNA; *mRNA*: Messenger RNA; *KH*: K-homology; *WT*: Wild type; *UTR*: Untranslated region; *IPTG*: Isopropyl β-d-1-thiogalactopyranoside; *BME*: Beta-mercaptoethanol; *PBS*: Phosphate Buffer Saline; *MMLV*: Moloney murine leukemia virus; *ROI*: Region of interest; *DTT*: Dithiotheritol; *PTM*: Post-translational modification

Supplementary Information The online version contains supplementary material available at https://doi.org/10.1007/s12035-022-03049-1.

Acknowledgements We thank Dr. Vinothkumar Kutti Ragunath (NCBS) for his useful comments and suggestions on the manuscript; Hitendra Negi (NCBS) for his help in our protein purification experiments; Sudhriti Ghosh Dastidar, CNS for his insights on FMRP and RPL10 puncta imaging and analysis; Central Imaging and Flow Cytometry Facility (CIFF) and Animal House Facility, NCBS-inStem; Members from the labs of Dr. Ravi Muddashetty, Dr .Dasaradhi Palakodeti, and Dr. Sumantra Chattarji (NCBS) for their invaluable suggestions and discussions.

Author Contribution M.N.D., S. Ramakrishna, S. Ravindran, D.N., and R.S.M.–designed the research; M.N.D., S. Ramakrishna, B.K.R., and V.J.–performed the research; L.Y. and D.N.–contributed to experimental tools; M.N.D., S. Ramakrishna, and D.N.–analyzed data; D.P. and R.S.M–provided funding; M.N.D–wrote the paper and M.N.D, S. Ramakrishna, S. Ravindran, B.K.R, V.J., L.Y., D.N, D.P., and R.S.M–reviewed versions of the manuscript.

Funding The work was supported by the NeuroStem grant (BT/IN/Denmark/07/RSM/2015–2016) awarded to Dr. Ravi S Muddashetty and the DST Swarnajayanti Fellowship (DST/SJF/LSA-02/2015–16) awarded to Dr. Dasaradhi Palakodeti. Deepak Nair acknowledges the Department of Biotechnology-Indian Institute of science partnership (DBT-IISc) program and Indian Institute of Science under Institute of Eminence (IISc-IOE) program for the research and infrastructure support. Michelle Ninochka D'Souza was supported by the DST-Inspire Fellowship (DST/INSPIRE Fellowship/2018/IF180201) from the Department of Science and Technology (DST).

Data Availability All data generated or analyzed during this study are included in this published article [and its supplementary information files.

Declarations

Ethics Approval All animal work was done in compliance with procedures approved by the Institutional Animal Ethics Committee (IAEC) and the Institutional Biosafety Committee (IBSC), InStem, Bangalore, India.

Consent to Participate Not applicable.

Consent for Publication All authors have given consent for submission of this manuscript.

Competing Interests The authors declare no competing interests.

References

1. Santoro MR, Bray SM, Warren ST (2012) Molecular Mechanisms of fragile X syndrome: a twenty-year perspective. Annu Rev Pathol Mech Dis 7(1):219–245
2. Myrick LK, Hashimoto H, Cheng X, Warren ST (2015) Human FMRP contains an integral tandem Agenet (Tudor) and KH motif in the amino terminal domain. Hum Mol Genet 24(6):1733–1740
3. Nelson DL, Orr HT, Warren ST (2013) The Unstable repeats—three evolving faces of neurological disease. Neuron 77(5):825–843
4. Siomi H, Siomi MC, Nussbaum RL, Dreyfuss G (1993) The protein product of the fragile X gene, FMR1, has characteristics of an RNA-binding protein. Cell 74(2):291–298
5. Hu Y, Chen Z, Fu Y, He Q, Jiang L, Zheng J et al (2015) The amino-terminal structure of human fragile X mental retardation protein obtained using precipitant-immobilized imprinted polymers. Nat Commun 6(1):6634
6. Alpatov R, Lesch BJ, Nakamoto-Kinoshita M, Blanco A, Chen S, Stützer A et al (2014) A Chromatin-dependent role of the fragile X Mental retardation protein FMRP in the DNA damage response. Cell 157(4):869–881
7. Antar LN (2004) Metabotropic glutamate receptor activation regulates fragile X Mental retardation protein and Fmr1 mRNA localization differentially in dendrites and at synapses. J Neurosci 24(11):2648–2655
8. Darnell JC, Van Driesche SJ, Zhang C, Hung KYS, Mele A, Fraser CE et al (2011) FMRP stalls ribosomal translocation on mrnas linked to synaptic function and autism. Cell 146(2):247–261
9. D'Souza MN, Gowda NKC, Tiwari V, Babu RO, Anand P, Dastidar SG, et al. (2018) FMRP Interacts with C/D box snoRNA in the nucleus and regulates ribosomal RNA methylation. iScience 9:399–411

10. Kute PM, Ramakrishna S, Neelagandan N, Chattarji S, Muddashetty Ravi S (2019) NMDAR mediated translation at the synapse is regulated by MOV10 and FMRP. Mol Brain 12(1):65
11. Muddashetty RS, Kelic S, Gross C, Xu M, Bassell GJ (2007) Dysregulated metabotropic glutamate receptor-dependent translation of AMPA receptor and postsynaptic density-95 mRNAs at synapses in a mouse model of fragile X syndrome. J Neurosci 27(20):5338–5348
12. Pasciuto E, Bagni C (2014) SnapShot: FMRP Interacting proteins. Cell 159(1):218-218.e1
13. Huber KM, Gallagher SM, Warren ST, Bear MF (2002) Altered synaptic plasticity in a mouse model of fragile X mental retardation. Proc Natl Acad Sci 99(11):7746–7750
14. Sidorov MS, Auerbach BD, Bear MF (2013) Fragile X mental retardation protein and synaptic plasticity. Mol Brain 6(1):15
15. Bear MF, Huber KM, Warren ST (2004) The mGluR theory of fragile X mental retardation. Trends Neurosci 27(7):370–377
16. Antar LN, Dictenberg JB, Plociniak M, Afroz R, Bassell GJ (2005) Localization of FMRP-associated mRNA granules and requirement of microtubules for activity-dependent trafficking in hippocampal neurons. Genes Brain Behav 4(6):350–359
17. Darnell JC (2005) Kissing complex RNAs mediate interaction between the fragile-X mental retardation protein KH2 domain and brain polyribosomes. Genes Dev 19(8):903–918
18. Feng Y, Absher D, Eberhart DE, Brown V, Malter HE, Warren ST (1997) FMRP Associates with polyribosomes as an mRNP, and the I304N mutation of severe fragile X syndrome abolishes this association. Mol Cell 1(1):109–118
19. Stefani G (2004) Fragile X mental retardation protein is associated with translating polyribosomes in neuronal cells. J Neurosci 24(33):7272–7276
20. Muddashetty RS, Nalavadi VC, Gross C, Yao X, Xing L, Laur O et al (2011) Reversible Inhibition of PSD-95 mRNA translation by miR-125a, FMRP phosphorylation, and mGluR signaling. Mol Cell 42(5):673–688
21. Narayanan U, Nalavadi V, Nakamoto M, Thomas G, Ceman S, Bassell GJ et al (2008) S6K1 phosphorylates and regulates fragile X Mental retardation protein (FMRP) with the neuronal protein synthesis-dependent mammalian target of rapamycin (mTOR) signaling cascade. J Biol Chem 283(27):18478–18482
22. Ceman S, O'Donnell WT, Reed M, Patton S, Pohl J, Warren ST (2003) Phosphorylation influences the translation state of FMRP-associated polyribosomes. Hum Mol Genet 12(24):3295–3305
23. Nalavadi VC, Muddashetty RS, Gross C, Bassell GJ (2012) Dephosphorylation-induced ubiquitination and degradation of FMRP in dendrites: a role in immediate early mGluR-stimulated translation. J Neurosci 32(8):2582–2587
24. Ferron L, Novazzi CG, Pilch KS, Moreno C, Ramgoolam K, Dolphin AC (2020) FMRP regulates presynaptic localization of neuronal voltage gated calcium channels. Neurobiol Dis 138:104779
25. Zhan X, Asmara H, Cheng N, Sahu G, Sanchez E, Zhang FX et al (2020) FMRP(1–297)-tat restores ion channel and synaptic function in a model of fragile X syndrome. Nat Commun 11(1):2755
26. Athar YM, Joseph S (2020) The Human fragile X Mental retardation protein inhibits the elongation step of translation through Its RGG and C-terminal domains. Biochemistry 59(40):3813–3822
27. Phan AT, Kuryavyi V, Darnell JC, Serganov A, Majumdar A, Ilin S et al (2011) Structure-function studies of FMRP RGG peptide recognition of an RNA duplex-quadruplex junction. Nat Struct Mol Biol 18(7):796–804
28. Laggerbauer B (2001) Evidence that fragile X mental retardation protein is a negative regulator of translation. Hum Mol Genet 10(4):329–338
29. Tekcan A (2016) In Silico analysis of FMR1 gene missense SNPs. Cell Biochem Biophys 74(2):109–127
30. Collins SC, Bray SM, Suhl JA, Cutler DJ, Coffee B, Zwick ME et al (2010) Identification of novel FMR1 variants by massively parallel sequencing in developmentally delayed males. Am J Med Genet 152A(10):2512–2520
31. Handt M, Epplen A, Hoffjan S, Mese K, Epplen JT, Dekomien G (2014) Point mutation frequency in the FMR1 gene as revealed by fragile X syndrome screening. Mol Cell Probes 28(5–6):279–283
32. Okray Z, Esch CE, Van Esch H, Devriendt K, Claeys A, Yan J et al (2015) A novel fragile X syndrome mutation reveals a conserved role for the carboxy-terminus in FMRP localization and function. EMBO Mol Med 7(4):423–437
33. Khatter H, Myasnikov AG, Natchiar SK, Klaholz BP (2015) Structure of the human 80S ribosome. Nature 520(7549):640–645
34. Fay DS, Gerow K. A biologist's guide to statistical thinking and analysis. In: WormBook: The Online Review of C. elegans Biology [Internet]. Pasadena (CA): WormBook; 2005–2018. Available from: https://www.ncbi.nlm.nih.gov/books/NBK153593/
35. Suvrathan A, Hoeffer CA, Wong H, Klann E, Chattarji S (2010) Characterization and reversal of synaptic defects in the amygdala in a mouse model of fragile X syndrome. Proc Natl Acad Sci 107(25):11591–11596
36. Pfeiffer BE, Huber KM (2007) Fragile X Mental retardation protein induces synapse loss through acute postsynaptic translational regulation. J Neurosci 27(12):3120–3130
37. Wang H, Dictenberg JB, Ku L, Li W, Bassell GJ, Feng Y (2008) Dynamic Association of the fragile X mental retardation protein as a messenger ribonucleoprotein between microtubules and polyribosomes. Wickens MP, editor. MBoC 19(1):105–14.
38. Darnell JC, Klann E (2013) The translation of translational control by FMRP: therapeutic targets for FXS. Nat Neurosci 16(11):1530–1536
39. Dieterich DC, Hodas JJL, Gouzer G, Shadrin IY, Ngo JT, Triller A et al (2010) In situ visualization and dynamics of newly synthesized proteins in rat hippocampal neurons. Nat Neurosci 13(7):897–905
40. Tsang B, Arsenault J, Vernon RM, Lin H, Sonenberg N, Wang LY et al (2019) Phosphoregulated FMRP phase separation models activity-dependent translation through bidirectional control of mRNA granule formation. Proc Natl Acad Sci USA 116(10):4218–4227
41. De Diego OY, Severijnen LA, van Cappellen G, Schrier M, Oostra B, Willemsen R (2002) Transport of fragile X Mental retardation protein via granules in neurites of PC12 Cells. Mol Cell Biol 22(23):8332–8341
42. Verkerk AJMH, Pieretti M, Sutcliffe JS, Fu YH, Kuhl DPA, Pizzuti A et al (1991) Identification of a gene (FMR-1) containing a CGG repeat coincident with a breakpoint cluster region exhibiting length variation in fragile X syndrome. Cell 65(5):905–914
43. Ascano M, Mukherjee N, Bandaru P, Miller JB, Nusbaum JD, Corcoran DL et al (2012) FMRP targets distinct mRNA sequence elements to regulate protein expression. Nature 492(7429):382–386
44. Brown V, Jin P, Ceman S, Darnell JC, O'Donnell WT, Tenenbaum SA et al (2001) Microarray Identification of FMRP-Associated brain mRNAs and Altered mRna translational profiles in Fragile X Syndrome. Cell 107(4):477–487
45. Chen E, Sharma MR, Shi X, Agrawal RK, Joseph S (2014) Fragile X Mental retardation protein regulates translation by binding directly to the ribosome. Mol Cell 54(3):407–417
46. Darnell JC, Van Driesche SJ, Zhang C, Hung KYS, Mele A, Fraser CE et al (2011) FMRP Stalls ribosomal translocation on mrnas linked to synaptic function and autism. Cell 146(2):247–261
47. Mateju D, Eichenberger B, Voigt F, Eglinger J, Roth G, Chao JA (2020) Single-molecule imaging reveals translation of mRNAs localized to stress granules. Cell 183(7):1801-1812.e13
48. Bechara EG, Didiot MC, Melko M, Davidovic L, Bensaid M, Martin P, et al. (2009) A Novel function for fragile X Mental

retardation protein in translational activation. Wickens M, editor. PLoS Biol 7(1):e1000016
49. Myrick LK, Nakamoto-Kinoshita M, Lindor NM, Kirmani S, Cheng X, Warren ST (2014) Fragile X syndrome due to a missense mutation. Eur J Hum Genet 22(10):1185–1189